# Hierarchical Colour-Shift-Keying Aided Layered Video Streaming for the Visible Light Downlink

Chuan Zhu, Yongkai Huo, Junyi Jiang, Hua Sun, Chen Dong, Rong Zhang and Lajos Hanzo, *Fellow, IEEE*
School of ECS, University of Southampton, UK.
Email: {cz12g09, yh3g09, jj4e09, hs4g09, cd2g09, rz, lh}@ecs.soton.ac.uk, http://www-mobile.ecs.soton.ac.uk

***Abstract*—Colour-shift keying (CSK) constitutes an important modulation scheme conceived for the visible light communications (VLC). The signal constellation of CSK relies on three different-colour light-sources invoked for information transmission. The CSK constellation has been optimized for minimizing the bit error rate, but no effort has been invested in investigating the feasibility of CSK aided unequal error protection (UEP) schemes conceived for video sources. Hence in this treatise, we conceive a hierarchical CSK (HCSK) modulation scheme based on the traditional CSK, which is capable of generating interdependent layers of signals having different error probability, which can be readily reconfigured by changing its parameters. Furthermore, we conceived a HCSK design example for transmitting scalable video sources with the aid of a recursive systematic convolutional (RSC) code. An optimisation method is conceived for enhancing the UEP and for improving the quality of the received video. Our simulation results show that the proposed optimized-UEP 16-HCSK-RSC system outperforms the traditional EEP scheme by about 1.7 dB of optical SNR at a peak signal-to-noise ratio (PSNR) of 37 dB, whilst optical SNR savings of up to 6.5 dB are attained at a lower PSNR of 36 dB.**

## I. Introduction

### A. Background of Visible Light Communication

This treatise is based on the structure of Fig. 1. Given the growing popularity of indoor multimedia applications, such as Voice over IP (VoIP), smart TV and online video games, video streaming substantially contributes to the exponentially increased amount of mobile data traffic. As a counter-measure, Heterogeneous Networks (HetNet) relying on smaller cells are relied upon, in order to achieve a higher system capacity for coping with the growing demands. However, the denser reuse of spectral resources will potentially impose an increased amount of interference [1]. In the light of these problems, Visible Light Communications (VLC) [2]–[6] has emerged as an appealing access method to provide extra license-free bandwidth, as a compliment to WiFi, femtocells, ultra wideband (UWB) and mm-wave communications in order to support indoor communications. Specifically, VLC supports high-rate downlink communications, in addition to its primary function of illumination in indoor environments. The recent IEEE standard 802.15.7 [5] on VLC also paves the way for wider commercial exploitation of VLC. The history of VLC systems is portrayed at a glance in Table I.

Colour-shift keying (CSK) relies on multiple light sources and photo-detectors corresponding to different colours, as introduced in the IEEE 802.15.7 standard, along with on-off Keying (OOK) and variable pulse position modulation

The financial support of the EPSRC under the contract EP/Noo4558/1 and EP/L018659/1 and that of the ERC's Advanced Fellow Grant and of the Royal Society's Research Merit Award is gratefully acknowledged.

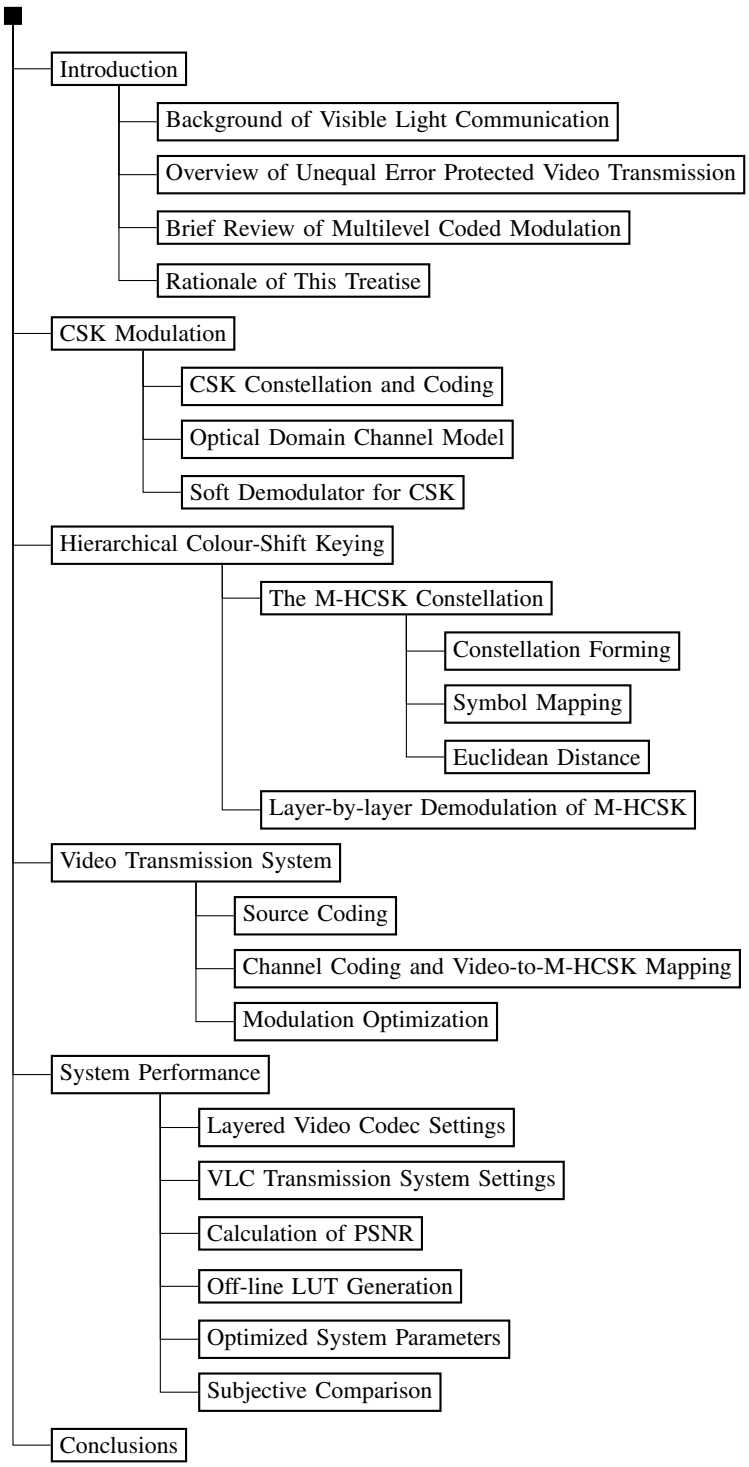


Figure 1: The structure of the paper

| Year | Authors/ Institutions | Contributions |
|---|---|---|
| 1999 | Pang *et al.* [7] | proposed high-switching-speed LEDs and their modulation for visible light communications. |
| 2000 | Tanakat *et al.* [8] | proposed white LED for both communications and illumination. |
| 2003 | Komine and Nakagawa [9] | designed a Power-Line Communication (PLC)/VLC system prototype. |
| | Visible Light Communications Consortium (VLCC) [10] | VLCC was established in Japan (http://www.vlcc.net/). |
| 2007 | VLCC [11] | proposed two standards: Visible Light Communication System Standard and Visible Light ID System Standard. |
| 2008 | European Union [12] | sponsored the Home Gigabit Access (OMEGA) project. |
| 2010 | LVX, Minnesota [13] | signed a contract with the city of St. Cloud, Minnesota, which is the first city to commercially deploy the VLC technology. |
| 2011 | IEEE 802.15 Working Group [5] | published IEEE 802.15.7 VLC standard. |
| | Li-Fi (Light-Fidelity) Consortium [14] | was formed in Oslo, Norway, as a complement to Wi-Fi. |
| 2014 | VLCA (Visible Light Communications Associations) [15] | is established as a successor of VLCC in Japan for further standardization of VLC. |

Table I: Major milestones in the history of VLC systems

| Year | Authors | Contributions |
|---|---|---|
| 1983 | Proakis *et al.* [23] | described On-Off Keying (OOK) and pulse amplitude modulation (PAM). |
| 1989 | Sugiyama *et al.* [24] | proposed multiple pulse position modulation (MPPM) to improve the bandwidth efficiency of PPM. |
| 1993 | Shalaby [25] | conceived overlapping PPM (OPPM). |
| 1998 | Ghassemlooy *et al.* [26] | proposed digital pulse interval modulation (DPIM) for optical wireless communication (OWC). |
| 1999 | Shiu *et al.* [27] | designed differential PPM (DPPM) for OWC. |
| 2003 | Ohtsuki [28] | proposed subcarrier-index modulation (SIM) for OWC. |
| 2007 | Fan *et al.* [29] | compared of PPM and pulse width modulation (PWM) for application in OWC. |
| 2010 | Nguyen *et al.* [30] | compared the bandwidth efficiency of MPPM with classic PPM. |
| 2011 | Rufo *et al.* [31] | compared to PPM with OOK at a given average power requirement in VLC systems. |
| 2012 | Arnon [32] | studied the effect of clock jitter using PPM in VLC applications. |
| 2013 | Fujimoto *et al.* [33] | demonstrated a low-cost high-speed VLC system using OOK-Non-return-to-zero (NRZ) signalling at 456 Mbit/s of data rate. |
| 2014 | Li *et al.* [34] | demonstrated the benefits of a VLC system using OOK-NRZ modulation for achieving a bitrate of 340 Mb/s in a bandwidth of 151 MHz. |
| | Chen and Chow [35] | demonstrated a multi-user VLC system using CSK and code-division multiple-access (CDMA) technology. |
| 2015 | Biagi *et al.* [36] | evaluated PPM relying on space time block coding in VLC systems. |

Table II: Major contributions on single carrier modulations for VLC systems

(VPPM). A compact historical portrayal of the modulation schemes designed for VLC systems is provided in Table II. Although the basic CSK modulation scheme was conceived in [5], recent research optimized it further for specific scenarios [16]–[20]. Drost and Sadler [17] examined the design of CSK signaling constellations conceived for an additive white Gaussian noise channel (AWGN) and optimized the location of the constellation points. In their follow-on work [18], VLC systems employing an arbitrary number of LEDs were investigated and they pre-compensated the channel effects at the transmitter. A new CSK modulation format based on four colours was presented in [19] by Singh *et al.*, while Monteiro and Hranilovic [21] set out to optimize high-order CSK constellations for specific communication channels. Finally, different signal labelling strategies were designed in [22] for diverse color constellations and detection schemes in order to improve the attainable Bit Error Ratio (BER) performance.

### *B. Overview of Unequal Error Protected Video Transmission*

Again, in order to satisfy the escalating mobile data demands, efficient video streaming should be considered for the sake of conceiving sophisticated transmission schemes. Layered video coding [37] is a widely used scheme designed for employment in heterogeneous networking problems. The concept of layered video coding relies on the provision of multiple layers of different importance, namely the base layer (BL), which conveys the most important video bits required for representing a low-resolution video, as well as the enhancement layers (ELs), which provide additional video quality refinements, when a higher channel quality allows their transmission. Therefore, layered video coding is capable of supporting different-resolution terminals having different quality-requirements, as shown in Fig. 2. It is also suitable for progressive reception of video steams according to the diverse network and channel conditions of different users. Therefore layered video coding is widely supported by the popular video standards [38]–[42]. Specifically, partitioned video coding [41] was provided by H.264 in order to generate multiple layers of different error-sensitivity. The Moving picture expert group (MPEG) provided the so-called multiview profile (MVP) [39], which generates different-angle encoded

camera-views as different layers. Scalable video coding (SVC) [40], [41] constitutes an extension of the H.264/AVC standard [41], and it generates an encoded stream containing multiple inter-dependent layers. Finally, an extension referred to as scalable high-efficiency video coding (SHVC) [43], [44] is being developed for the state-of-the-art high efficiency video coding (HEVC)/H.265 scheme [38], in order to support flexible scalability.

Due to the fact that the different video layers typically exhibit a distinct level of importance in terms of their contributions to the quality of the recovered video, unequal error protection (UEP) [48] constitutes a promising technique of conveying the video streams through noisy channels. More specifically, UEP can be achieved by using specific forward error correction (FEC) schemes carefully combined with particular modulation or coded modulation schemes. In the context of UEP schemes, either the packet-level regimes [49]–[56] or the bit-level schemes [47], [55], [57]–[63] may be adopted. The packet-level contributions of [49]–[53], [64]–[66] refer to the schemes, where hard decoded FEC codes, e.g. Reed-Solomon (RS) codes or Luby transform (LT) codes are invoked for mitigating the packet loss events at the application layer [67]. By contrast, the bit-level arrangements operate at the physical layer and rely on soft-decoded FEC codes for correcting bit-errors in wireless scenarios [47], [68], [69]. Specifically, the authors of [47] proposed a bit-level inter-layer coded FEC (IL-FEC) scheme that embeds the BL into the FEC coded ELs, so that the reception of the BL can be improved with the aid of the ELs using soft decoding. The schematic of the proposed IL-FEC is shown in Fig. 3. For the reader's convenience, we have assembled the major contributions on UEP for video communications in Table III.

### C. Brief Review of Multilevel Coded Modulation

To elaborate a little further, UEP can also be achieved by appropriately designing modulation and coded modulation schemes [59], [72], [77], [78], [81], [84], [85], [87]–[98]. Both multilevel coded (MLC) modulation [59], [72], [90]–[93] and hierarchical modulation (HM) [77], [78], [81], [84], [85], [87], [94]–[98] have attracted substantial research attention, albeit the latter one can be considered as a special subset of the former one. Multilevel coded modulation was originally proposed by Calderbank and Seshadri for providing UEP [72], where the 2-dimensional signal constellation is partitioned into disjoint subsets and the bit streams of different importance are carefully mapped to the different-integrity bit-positions of the constellation subsets. Later the theoretical upper bounds and the computer simulation-based performance of multilevel block coded modulations designed for UEP and multistage decoding were presented in [90], [91]. Aydinlik and Salehi [59], as well as Kim *et al.* [92] improved the set partitioning of QAM used by TCM to achieve an improved UEP performance. Finally, a multilevel space-shift-keying scheme was designed by Zamkotsian *et al.* [93] to provide UEP for transmission over Rician fading channels.

Again, HM is another popular UEP technique that has already been widely accepted by industry and hence became an integral part of the DVB-T/-H standard [104], [105]. Similar to MLC modulation, the symbols of the HM schemes are carefully partitioned into different-integrity groups. Since the different bits in a symbol are used for selecting specific subgroups of the constellation points, they have different error probabilities. HM has also been investigated in the context of cooperative communications, where the different-priority layers can be routed via different paths [101]–[103], [106].

Numerous systems have been developed for UEP by exploiting the properties of HM schemes. To elaborate, an UEP system was proposed by Chang *et al.* [84] to support multiple protection levels, instead of the traditional twin-level designs. HM based on QAM was investigated as the UEP modulation method [107]. The authors of [94], [96], [97] proposed HM-QAM-style MIMO systems and analysed the attainable UEP properties. However, the authors of [94], [96], [97] carried out their investigations without actually considering multimedia sources. By contrast, the authors of [95] jointly optimised the channel coding parameters and the HM parameters in a coded-HM-aided progressive image transmission system, in order to minimize the video distortion. The streaming of partition-mode H.264/AVC [41] coded video was considered in [77] and UEP was provided by the HM-QAM scheme for protecting the video partitions of different importance. Similarly, H.264 coded video was also considered by Chang *et al.* [78], where the intra-coded frames (I-frame) and predictive coded frames (P-frame) were protected using different levels of protection provided by adaptive HM-QAM. Li *et al.* [81] conceived an UEP scheme for transmitting H.264 coded video over frequency selective fading channels, using OFDM-based HM-QAM for carefully mapping the video bits to the OFDM-subcarriers to provide the video layers of high importance with better error protection. Finally, depth-map based stereoscopic video streaming was considered using HM 16-QAM in [85]. Since the color component of the video sequence has a more significant impact on the reconstructed video quality than the depth map, the color-component of the 3D video was mapped to the layers of better protection in the HM-QAM scheme. A brief review of the major contributions on UEP schemes using MLC and HM can be found in Table IV.

### D. Rationale of This Treatise

Although VLC offers a large bandwidth for data transmission [108], and the current standard supports a data rate of 48 Mb/s (or 384 Mbps) when CSK is combined with channel coding [5], there is a surging demand for higher data transmission rates for applications like the streaming of 4K or higher-resolution videos, which may have data-rates of hundreds of Mbps [109]. Additionally, multiple-user and multiple-source scenarios [35], [110], [111] also require higher data rates. Finally, the received SNR of the indoor VLC systems dramatically drops, when the receiver does not have a clear line of sight to the lighting system [108], [112]. Therefore, it is necessary to protect the system against any video performance degradation due to dropping some of the video-layers during indoor VLC transmission. In order to maintain the maximum possible video quality in the presence of error-prone video data, UEP is adopted by using hierarchical modulation in our treatise.

Despite the rich research efforts invested in optimizing the CSK constellation for reducing the BERs, no efforts have

| Year | Author(s) | Contribution |
|---|---|---|
| 1967 | Masnick and Wolf [70] | proposed the concept of UEP, which protects more important data with the aid of stronger FEC. |
| 1988 | Hagenauer [71] | investigated a UEP system using rate-compatible punctured convolutional (RCPC) codes. |
| 1993 | Calderbank and Seshadri [72] | proposed multilevel codes for UEP. |
| 1996 | Albanese *et al.* [73] | proposed priority encoded transmission (PET) scheme for sending messages over lossy packet-based networks by exploiting their specific priorities. |
| 2000 | Wu *et al.* [67] | proposed a packet-level UEP scheme employing hard decoded FEC codes for mitigating the packet loss events at the application layer. |
| 2001 | Chou *et al.* [74] | proposed a layered multicast system of audio and video using PET. |
| 2003 | Stockhammer *et al.* [68] | proposed a bit-level UEP for transmitting H.264/AVC coded video in wireless environments. |
| 2004 | Zhang *et al.* [75] | designed a HARQ scheme to provide UEP for video transmission by appropriately sharing the bitrate budget between the source and channel encoders. |
| 2005 | Brüggen and Vary [76] | conceived an UEP scheme relying on specific power-allocation according to the bit error sensitivity of different transmitted data. |
| | Barmada *et al.* [77] | proposed a video transmission scheme for partitioned H.264/AVC coded video using HM-QAM to provide UEP. |
| 2006 | Chang *et al.* [78] | invoked an UEP scheme, where the intra/inter-coded frame of the H.264 coded video are protected using different levels of protection provided by adaptive hierarchical QAM. |
| 2007 | Rahnavard *et al.* [79] | proposed an UEP scheme provided by low-density parity-check (LDPC) codes. |
| 2009 | Park *et al.* [80] | conceived a UEP scheme for transmission SVC over an orthogonal frequency-division multiplexing (OFDM) channel. |
| 2010 | Li *et al.* [81] | designed an UEP scheme to transmit the H.264 coded video over frequency selective fading channels, combining hierarchical QAM combined with sub-carrier mapping to provide UEP. |
| 2011 | Arslan *et al.* [82] | optimised a coded progressive image transmission system. |
| | Hellge *et al.* [55] | proposed a UEP scheme for transmission over mobile channels by exploiting the hierarchy of video layers. |
| 2012 | Khalek *et al.* [83] | introduced an APP/MAC/PHY cross-layer UEP architecture for improving the perceptual quality of delay-constrained scalable video transmission. |
| | Chang *et al.* [84] | proposed a Hierarchical Modulation (HM) based system providing multiple levels of UEP. |
| | Alajel *et al.* [85] | conceived an UEP system for color plus depth-map aided stereoscopic video using hierarchical 16-QAM. |
| 2014 | Wu *et al.* [86] | proposed cross-layer-operation aided of UEP schemes for video transmission by using UEP Raptor codes at the application layer, and UEP RCPC codes at the physical layer. |
| | Nguyen *et al.* [87] | investigated the performance of UEP in wireless relay networks. |

Table III: Major contributions on unequal error protection for video communications.

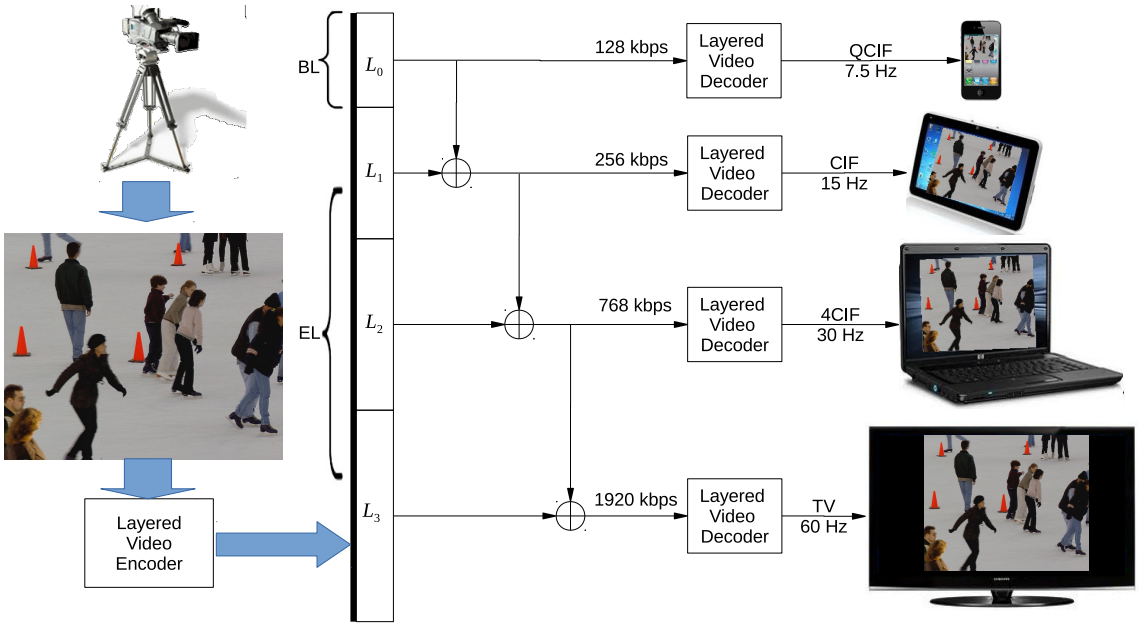


Figure 2: Streaming and decoding structure of a layered video [37], [45]

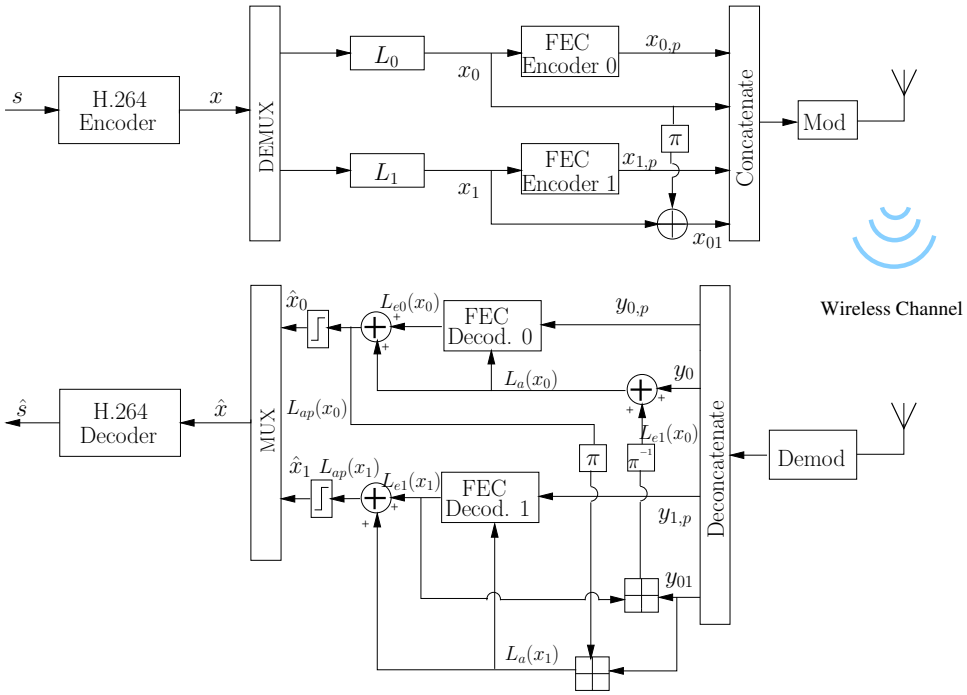


Figure 3: IL-FEC encoding architecture of layered video with two layers. [46], [47]

been dedicated to investigating the feasibility of UEP CSK schemes. Furthermore, no CSK-aided video systems have been disseminated in the open literature. Hence our inspiration is to close this open problem.

Explicitly, the rationale and novelty of this paper is summarized as follows.

1) We conceive a hierarchical CSK (HCSK) modulation constellation that can be readily configured to provide different error probabilities for the different video layers. We are the first to introduce HM into the conventional CSK constellations [16]–[20] and to design an UEP scheme based on it. The constellation and bit-to-symbol mapping of the traditional CSK are completely redesigned in our novel HCSK.
2) We provide a HCSK design example for transmitting scalable video sources relying on the RSC code as the FEC.
3) Our optimisation metric is the quality of the received video. We will demonstrate that the proposed system outperforms the traditional EEP scheme by about 1.7 dB of optical SNR at a video peak signal-to-noise ratio (PSNR) of 37 dB and up to 6.5 dB at a PSNR of 36 dB.

The rest of this paper is organized as follows. Section II introduces the CSK transmitter and receiver model, including the signal constellation and coding, the optical domain

| Year | Authors | Contributions |
|---|---|---|
| 1993 | Calderbank *et al.* [72] | first proposed multilevel coded modulation for providing UEP. |
| 1995 | Morimoto *et al.* [99] | designed a hierarchical modulation scheme for satellite communication. |
| 1996 | Morimoto *et al.* [100] | proposed hierarchical image transmission for multimedia mobile communications. |
| 2000 | Morelos *et al.* [91] | presented the theoretical upper bounds of multilevel block coded modulation designed for UEP and multistage decoding. |
| | Isaka *et al.* [90] | |
| 2001 | Kim and Pottie [92] | improved the set partitioning of QAM used by TCM to improve UEP performance. |
| 2005 | Barmada *et al.* [77] | proposed HM-QAM UEP for the streaming of partitioned H.264/AVC [41] coded video. |
| 2006 | Hossain *et al.* [101] | proposed an UEP scheme for voice and data transmission over fading channels using adaptive hierarchical modulation. |
| | Chang *et al.* [78] | designed an UEP scheme for H.264 coded video streaming, where I-frame and P-frame protected using different levels of protection provided by adaptive HM-QAM. |
| 2007 | Noh *et al.* [96] | proposed UEP-aided MIMO-OFDM systems relying on hierarchical signal constellations. |
| 2008 | Aydinlik and Salehi [59] | improved the set partitioning of QAM to achieve an improved UEP performance. |
| 2009 | Chang *et al.* [102] | derived the explicit closed-form expressions of the BER for cooperative communication systems combined with HM. |
| 2010 | Li *et al.* [81] | conceived an UEP scheme for transmitting H.264 coded video over frequency selective fading channels, using OFDM-based HM-QAM. |
| 2011 | Arslan *et al.* [95] | optimised the channel coding parameters and the HM parameters in a coded HM-aided progressive image transmission system. |
| 2012 | Chang *et al.* [94] | proposed HM-based space shift keying (SSK)-type modulation for UEP. |
| | Alajel *et al.* [85] | proposed HM-QAM for depth-map based stereoscopic video streaming. |
| 2014 | Zamkotsian *et al.* [93] | designed a multilevel space-shift-keying scheme to provide UEP for transmission over Rician fading channels. |
| | Quazi and Xu [97] | proposed HM-QAM-style MIMO systems and analysed the attainable UEP properties. |
| 2015 | Sun *et al.* [103] | investigated triple-layer turbo-trellis-coded HM in the context of cooperative communications. |

Table IV: Major contributions on UEP schemes using MLC or HM

channel model as well as the soft demodulation method. We then introduce the construction of our novel M-HCSK modulation and its layered demodulation method in Section III. We continue by optimizing a UEP system using M-HCSK-RSC transmission to convey scalable video sequences, as detailed in Section IV. The performance of our optimised M-HCSK-RSC video transmission system using different HCSK constellation sizes is compared to the relevant benchmarker schemes in Section V using different video sequences. Finally, we conclude in Section VI.

## II. CSK Modulation

In this section we will briefly describe the basics of CSK modulation that are associated with the transceiver architecture of Fig. 4. Specifically, we will describe the constellation of the CSK modulation, the channel model of the optical-domain propagation and the corresponding demodulation methods.

### A. CSK Constellation and Coding

As shown in Fig. 4, the bit sequence $\mathbf{b}$ is modulated on to the CSK symbols. For the $M$-ary CSK modulation, every group of $N_b = \log_2 M$ incoming bits, denoted by $\mathbf{b}_s$, is mapped to an $M$-ary CSK symbol. According to the IEEE 802.15.7 standard [5], the CSK symbols are modulated using the combination of three distinct sources of visible lights, having different wavelength/frequencies. Therefore the CSK symbols are represented by the three-dimensional vectors containing the intensities of the three components of the light. Explicitly, given a CSK symbol $\mathbf{s}$, it can be represented by $\mathbf{s} = [s_i, s_j, s_k]$, $\mathbf{s} \in \mathcal{S}$, where each element represents the power of the corresponding light source and $\mathcal{S} = \{\mathbf{s}_0, \mathbf{s}_1, \ldots, \mathbf{s}_{M-1}\}$ is the collection of all the $M$ legitimate symbols in $M$-ary CSK. According to the standard [5], the output light intensity of each of the light sources should be limited, i.e. we have

$$0 < s_p < I \tag{1}$$

for $p = i, j, k$. Furthermore, in most applications the total intensity of the CSK symbol must be constant, which is expressed as:

$$\sum_{p=i,j,k} s_p = I \quad . \tag{2}$$

Therefore, in a three dimensional space, the legitimate CSK symbols are confined to a triangular area on the $\sum_p s_p = I$ plane, as defined by the borderlines $\begin{cases} s_i + s_j & = I \\ s_k & = 0 \end{cases}$, $\begin{cases} s_i + s_k & = I \\ s_j & = 0 \end{cases}$ and $\begin{cases} s_j + s_k & = I \\ s_i & = 0 \end{cases}$, as shown in Fig. 5. Usually the symbol intensities $s_p$ are normalized by setting the intensity boundary $I$ to unity.

Observe that due to the additional constraint formulated in Eq. 2, the above-mentioned three dimensional representation of the CSK symbols only has two degrees of freedom. In fact the CSK symbols may also be represented by the CIE 1931 colour space [113], which uses the 2-dimensional vector of $\mathbf{q} = [x, y]$ to represent $s$. In the 2-dimensional representation, the three light components we used, i.e$[1, 0, 0]$, $[0, 1, 0]$ and $[0, 0, 1]$, which correspond to the three vertices of the triangular

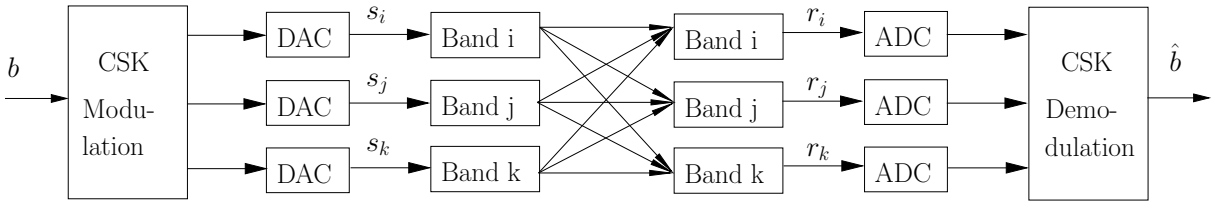


Figure 4: Transceiver architecture of a basic $M$-CSK transceiver

| Wavelength Band [nm] | Band | Centre [nm] | $(x, y)$ | $\mathbf{b}_s$ | $[s_\mathrm{i}, s_\mathrm{j}, s_\mathrm{k}]$ |
|---|---|---|---|---|---|
| 380 - 478 | Band k ($s_0$) | 429 | (0.169,0.007) | 1 0 | [0 0 1] |
| 540 - 588 | Band j ($s_1$) | 564 | (0.402,0.597) | 0 0 | [0 1 0] |
| 726 - 780 | Band i ($s_2$) | 753 | (0.734,0.265) | 1 1 | [1 0 0] |
| - | $s_3$ | - | (0.435,0.290) | 0 1 | [0.333 0.333 0.333] |

Table V: The information-carrying colours of 4-CSK modulation specified by the IEEE standard, where the constellation point $s_3$ is constituted by a weighted mixture of the red, yellow and blue colours © IEEE [5].

| Wavelength Band [nm] | Band | Centre [nm] | $(x, y)$ | $\mathbf{b}_s$ | $[s_\mathrm{i}, s_\mathrm{j}, s_\mathrm{k}]$ |
|---|---|---|---|---|---|
| 380 - 478 | Band k ($s_0$) | 429 | (0.169,0.007) | 1 0 0 1 | [0 0 1] |
| 540 - 588 | Band j ($s_1$) | 564 | (0.402,0.597) | 0 0 0 0 | [0 1 0] |
| 726 - 780 | Band i ($s_2$) | 753 | (0.734,0.265) | 1 0 0 0 | [1 0 0] |
| - | $s_3$ | - | (0.324,0.400) | 0 1 1 0 | [0.333 0.334 0.332] |
| - | $s_4$ | - | (0.413,0.495) | 0 0 0 1 | [0.111 0.779 0.115] |
| - | $s_5$ | - | (0.513,0.486) | 0 1 0 1 | [0.334 0.666 0] |
| - | $s_6$ | - | (0.335,0.298) | 0 0 1 0 | [0.110 0.445 0.445] |
| - | $s_7$ | - | (0.524,0.384) | 0 1 1 1 | [0.445 0.444 0.111] |
| - | $s_8$ | - | (0.247,0.204) | 1 0 1 0 | [0.0004 0.334 0.6656] |
| - | $s_9$ | - | (0.435,0.290) | 0 1 1 0 | [0.333 0.334 0.333] |
| - | $s_{10}$ | - | (0.623,0.376) | 0 1 0 0 | [0.666 0.334 0] |
| - | $s_{11}$ | - | (0.258,0.101) | 1 0 1 1 | [0.112 0.110 0.777] |
| - | $s_{12}$ | - | (0.446,0.187) | 1 1 1 0 | [0.445 0.111 0.445] |
| - | $s_{13}$ | - | (0.634,0.273) | 1 1 0 1 | [0.777 0.111 0.112] |
| - | $s_{14}$ | - | (0.357,0.093) | 1 1 1 1 | [0.3327 0.0003 0.667] |
| - | $s_{15}$ | - | (0.546,0.179) | 1 1 0 0 | [0.667 0 0.333] |

Table VI: The information-carrying colours of 16-CSK modulation specified by the IEEE standard, where the constellation points $s_3$ - $s_{15}$ are constituted by the weighted mixture of the red, yellow and blue colours © IEEE [5].

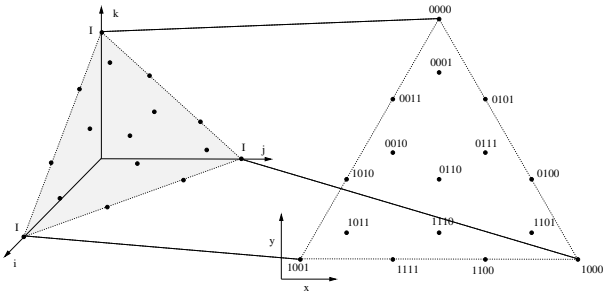


Figure 5: Colour constellations of 16-CSK without considering white balance, where the operating intensity is normalised to 1

area of the legitimate CSK symbols, are mapped into the new coordinates of $\mathbf{v}_i = [x_i, y_i]$, $\mathbf{v}_j = [x_j, y_j]$ and $\mathbf{v}_k = [x_k, y_k]$, respectively. Therefore the following equations may be used for defining the new 2-dimensional symbols:

$$\begin{aligned} x &= s_i x_i + s_j x_j + s_k x_k \\ y &= s_i y_i + s_j y_j + s_k y_k \end{aligned}, \tag{3}$$

which can also be formulated as:

$$\mathbf{q} = s_i \mathbf{v}_i + s_j \mathbf{v}_j + s_k \mathbf{v}_k, \tag{4}$$

and each vector $\mathbf{s}$ can be mapped to a unique vector $\mathbf{q}$, as shown in Fig. 5. The coordinates $\mathbf{v}_i$, $\mathbf{v}_j$ and $\mathbf{v}_k$ of the 2-dimensional vertices are also referred to as the centre of colour bands, and a total of 7 predefined settings were specified by the standard [5]. As the terminology suggests, each of them corresponds to a certain band of frequencies' colours. According to [5], there are only 9 valid colour band combinations consist a legitimate triangles. The points on the colour plane represent the CSK symbols generated by modulating the intensities of different colours of the legitimate colour band combinations on a RGB chip. For instance, the components are mapped to the Red, Yellow and Blue (RYB) LED transmitters according to the mapping scheme of Table V. Explicitly, for the corner

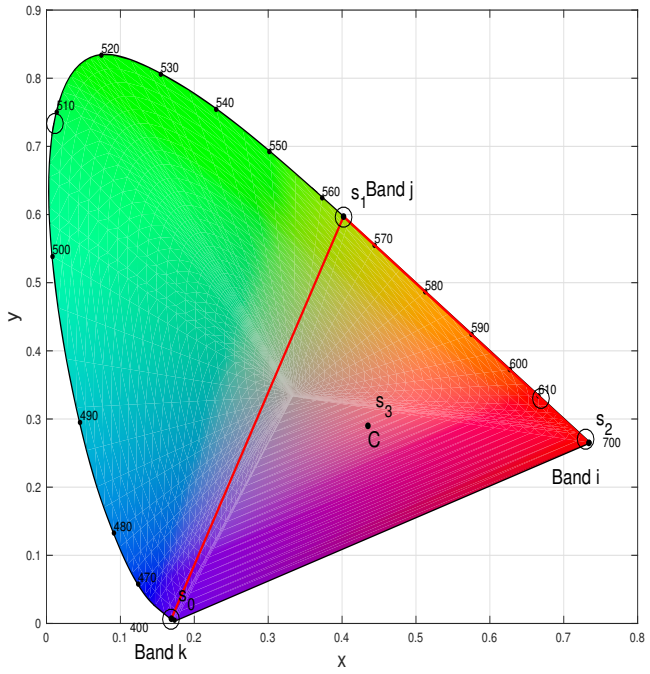


Figure 6: The CIE1931 colour plane for CSK modulation IEEE, where point (C) in the centroid of the triangle. The point $s_3$ and the three corner points represent four wavelength conveying 2 bits/symbol in 4-ary CSK © IEEE [5].

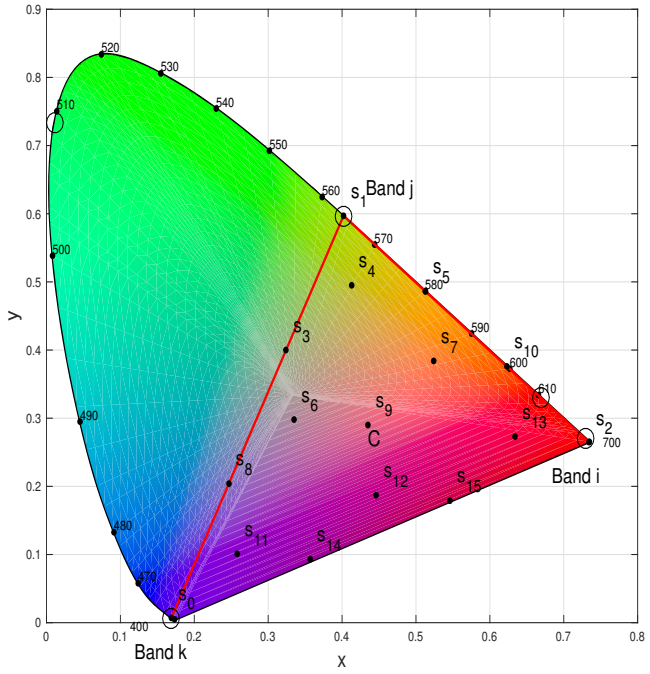


Figure 7: The CIE1931 colour plane for CSK modulation IEEE, where point (C) in the centroid of the triangle. The point $s_3$ - $s_{15}$ and the three corner points represent sixteen wavelength conveying 4 bits/symbol in 16-ary CSK © IEEE [5].

points of the triangle seen in Fig. 6, only one of the RYB LEDs is activated, as also seen in Table V, but for the point $s_3$, all of the RYB LEDs are activated according to the weights seen at the bottom right corner of Table V. As expected, these weights add up to unity. In analogy to classic Frequency Shift Keying (FSK), which detects the energy at the output of the detection filters, here the PDs detect the different visible-light colours falling into the 400 - 800 [THz] band. This justifies the terminology of CSK.

In IEEE 802.15.7 [5], the constellation settings are provided for 4-CSK, 8-CSK and 16-CSK. We can find the definition of symbol points for 4-CSK and 16-CSK in Fig. 8. For 4-CSK, we can observe in Fig. 8a that three symbol points are exactly on location of the vertices $\mathbf{v}_i$, $\mathbf{v}_j$ and $\mathbf{v}_k$ of the triangle, while the fourth symbol is at the centroid of the triangle. This design maximizes the Euclidean distances of the 4-CSK symbol points. For the 16-CSK constellation design of Fig. 8b, we can see that the entire triangular area is divided into 9 smaller triangles, which are congruent with each other and have $1/3$ of the edge-length of the original triangle. As many as 10 of the 16-CSK symbol points are on the vertices of these smaller triangles, while the remaining 6 of them are the centroids of 6 of the the smaller triangles that share at least one side with the entire triangle. Furthermore, if we join the constellation points "0010", "0111" and "1110" together, we will obtain a new small triangle that has the centroid of "0110" and it is congruent with the other small triangles. Therefore the constellation points of 16-CSK can simply be divided into the vertices and centroids of four congruent small triangles, where each setting of the 4 symbol points in each small triangle is similar to the 4-CSK symbol settings. We will further explore this interesting property later in this treatise.

The two-dimensional colour coordinates $\mathbf{q} = (x, y)$ of the symbols are generated by the intensity of the three light sources $\mathbf{s} = [s_\mathrm{i}, s_\mathrm{j}, s_\mathrm{k}]$, which represents the power of the light source. Therefore we can readily obtain the intensity vector $\mathbf{s}$ transmitted from the two-dimensional colour coordinates $\mathbf{q}$, under the settings of Table V and Table VI. Here we illustrate the conversion using 2 examples:

*Example 1*: For the 4-CSK modulation, given Band i, j and k of the CIE1931 colour plane of Fig. 6, the basic coordinates of the source colours RYB are $\mathbf{q}_R = \mathbf{v}_i$ = [0.734,0.265], $\mathbf{q}_Y = \mathbf{v}_j$ = [0.402,0.597] and $\mathbf{q}_B = \mathbf{v}_k$ = [0.169,0.007]. Then, to generate the specific colour at the point $s_3$ represented by $(x, y) = (0.435, 0.290)$ in Fig. 6, the intensity vector $\mathbf{s} = [s_\mathrm{i}, s_\mathrm{j}, s_\mathrm{k}]$ is obtained by solving the following equation:

$$\begin{cases} 0.435 = 0.734 s_\mathrm{i} + 0.402 s_\mathrm{j} + 0.169 s_\mathrm{k} \\ 0.290 = 0.265 s_\mathrm{i} + 0.597 s_\mathrm{j} + 0.007 s_\mathrm{k} \\ s_\mathrm{i} + s_\mathrm{j} + s_\mathrm{k} = 1, \end{cases} \tag{5}$$

where the resultant intensity vector becomes $\mathbf{s} = [s_\mathrm{i}, s_\mathrm{j}, s_\mathrm{k}]$ = [0.333049 0.334023 0.332928]. The intensity vector of other colour constellation points may be obtained in the same way, which has also been listed in Table V.

*Example 2*: For the 16-CSK modulation, the basic coordinates of the source colours RYB for Band i, j and k are still $\mathbf{q}_R = \mathbf{v}_i$ = [0.734,0.265], $\mathbf{q}_Y = \mathbf{v}_j$ = [0.402,0.597] and $\mathbf{q}_B = \mathbf{v}_k$ = [0.169,0.007]. The constellation points of 16-CSK modulation on the CIE 1931 colour plane are shown in Fig. 7, which are represented by the two-component colour

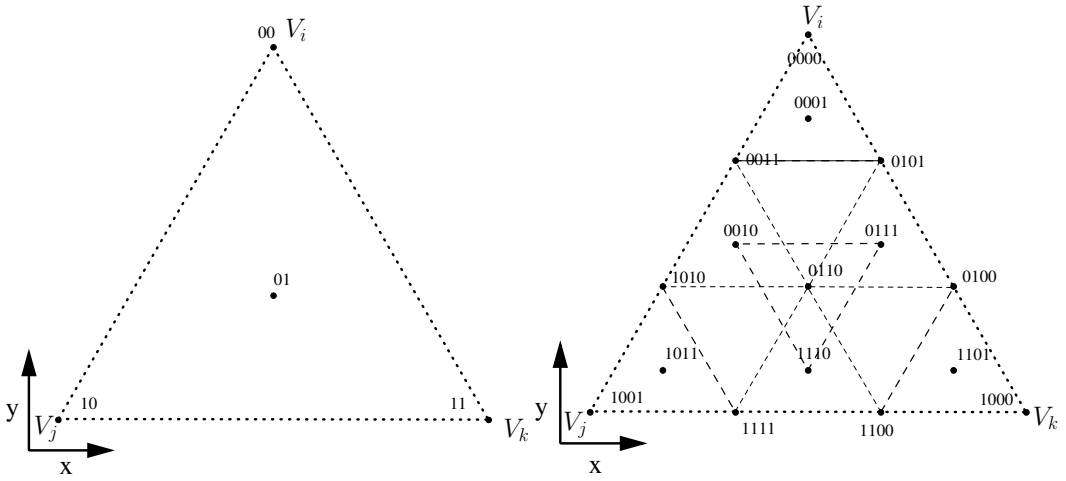


(a) Constellation for 4-CSK (b) Constellation for 16-CSK

Figure 8: Constellation for 4-CSK and 16-CSK in IEEE 802.15.7 [5]

coordinates and three-component intensity vectors listed in Table VI. For example, the two-component coordinates of point $s_{12}$ are represented by $(x, y) = (0.446, 0.187)$ in Fig. 7, which the intensity vector $\mathbf{s} = [s_{\rm i}, s_{\rm j}, s_{\rm k}]$ is obtained by

$$\begin{cases} 0.446 = 0.734s_{\rm i} + 0.402s_{\rm j} + 0.169s_{\rm k} \\ 0.187 = 0.265s_{\rm i} + 0.597s_{\rm j} + 0.007s_{\rm k} \\ s_{\rm i} + s_{\rm j} + s_{\rm k} = 1. \end{cases} \tag{6}$$

Hence, the resultant intensity vector becomes $\mathbf{s} = [s_{\rm i}, s_{\rm j}, s_{\rm k}]$ = [0.445, 0.444, 0.111], as shown in Table VI.

Hence to summarize, the conversion of two-dimensional colour coordinates $\mathbf{q} = (x, y)$ of the symbol to the three-dimensional optical signal intensity $\mathbf{s} = [s_{\rm i}, s_{\rm j}, s_{\rm k}]$ is achieved by simultaneously solving a simple system of three equations, which is given by Eq. (2) and Eq. (4). Here we define the coordinate-vector of the three light sources as $\mathbf{v}_i$, $\mathbf{v}_j$ and $\mathbf{v}_k$. Thus the entire CSK modulation process may be interpreted as a one-to-one mapping function.

### *B. Optical Domain Channel Model*

As shown in Fig. 4, the modulated CSK symbol $\mathbf{s}$ is transmitted with the aid of 3 different light sources, and received by three separate Photon-Detectors (PD), which convert the intensities of light into electronic signals. The optical domain channel of Fig. 4 is represented with a noisy multipath model, which characterizes the channel-induced degradations, such as the multi-color imbalance, multi-color interference, ambient light-induced noise, as well as device noise. The contaminated received signal $\hat{\mathbf{s}} = [\hat{s}_i, \hat{s}_j, \hat{s}_k]$ can be represented as

$$\hat{\mathbf{s}} = \mathbf{H}\mathbf{s}^T + \mathbf{n}^T, \tag{7}$$

where $\mathbf{H}$ is a $(3 \times 3)$-element matrix, which is represented as

$$\mathbf{H} = \begin{bmatrix} h_{ii} & h_{ji} & h_{ki} \\ h_{ij} & h_{jj} & h_{kj} \\ h_{ik} & h_{jk} & h_{kk} \end{bmatrix}. \tag{8}$$

Each element represents the channel gain between a specific light source and a PD, $h_{ij}$ for example is the channel gain between the light source $i$ and PD $j$, representing the interference imposed. In this treatise we consider the non-dispersive AWGN channel, where $\mathbf{H}$ is simply an identity matrix, while $\mathbf{n} = [n_i, n_j, n_k]$ is the AWGN noise vector having a total power of $\sigma^2$, with each element having the power of $\sigma_0^2 = \sigma^2/3$. The variance $\sigma_0^2$ of the AWGN at each of the PDs, can be modelled as

$$\sigma_0^2 = \sigma_{\rm S}^2 + \sigma_{\rm T}^2, \tag{9}$$

according to [19], where the shot noise variance $\sigma_{\rm S}^2$ is defined by

$$\sigma_{\rm S}^2 = 2qR\left(P_{Signal}\left(t\right) + P_{Daylight}\right)W \tag{10}$$

and the thermal noise variance $\sigma_{\rm T}^2$ is given by

$$\sigma_{\rm T}^2 = \frac{4k_BTW}{r}, \tag{11}$$

where $W$ is the bandwidth, $q$ is the charge of an electron, $R$ is the responsivity of PD, $P_{Signal}\left(t\right)$ is the instantaneous received power, $P_{Daylight}$ is the mean power received from the diffuse sunlight in indoor environments, $k_B$ is Boltzmann's constant and $T$ is the temperature of the noise equivalent input resistance $r$ in Kelvin. By substituting $\sigma_{\rm S}^2$ and $\sigma_{\rm T}^2$ in Eq. (9) we arrive at

$$\sigma_0^2 = 2\left(qRP_{Signal}\left(t\right) + qRP_{Daylight} + \frac{2k_bT}{r}\right)W. \tag{12}$$

In the scenario of an indoor office environment [19], the lighting provides approximately 400 lux of illuminance, while the daylight is about 50 lux at the centre of the office. Therefore $P_{Daylight}$ is assumed to be approximately 11% of the mean value of $P_{Signal}\left(t\right)$ according to [19].

Hereby we define the optical SNR as $\gamma_o = E_s/\sigma^2$, and $E_s = \mathbb{E}\left\{||\mathbf{s}||^2\right\}$, which is the average of the power of all possible $M$-ary CSK symbols.

### *C. Soft Demodulator for CSK*

Basically, a simple estimate of $\mathbf{s}$, denoted by $\hat{\mathbf{s}}$, can be obtained by compensating the propagation-induced impairment reflected by $\mathbf{H}$ [5]:

$$\hat{\mathbf{s}} = \mathbf{H}^{-1}\mathbf{r}. \tag{13}$$

However, to fully exploit the information for post-demodulation decoding, we have to obtain the *a posteriori* probability of each symbol $\mathbf{s}_m$, $\mathbf{s}_m \in \mathcal{S}$, which can be readily expressed as:

$$\begin{aligned}\Pr(\mathbf{s}_m|\mathbf{r}) &= \mathrm{p}(\mathbf{r}|\mathbf{s}_m)\frac{\Pr(\mathbf{s}_m)}{\mathrm{p}(\mathbf{r})} \\ &= \frac{\Pr(\mathbf{s}_m)}{2\pi\sigma \mathrm{p}(\mathbf{r})}\exp\left(-\frac{\|\mathbf{r}-\mathbf{H}\mathbf{s}_m\|^2}{2\sigma^2}\right),\end{aligned} \tag{14}$$

where $\Pr(\mathbf{s}_m)$ is the *a priori* probability of the symbol $\mathbf{s}_m$. For simplicity, Eq. (14) can be expressed in the log domain as

$$\mathrm{lr}(\mathbf{s}_m|\mathbf{r}) = A - \left(\|\mathbf{r}-\mathbf{H}\mathbf{s}_m\|^2/2\sigma^2\right), \tag{15}$$

where $A = \ln[\Pr(\mathbf{s}_m)] - \ln[2\pi\sigma \mathrm{p}(\mathbf{r})]$ and $A$ is the same for all $\mathbf{s}_m$ when no *a priori* information is provided, while $\mathrm{lr}(\mathbf{s}_m|\mathbf{r})$ is defined as $\ln[\Pr(\mathbf{s}_m|\mathbf{r})]$.

At this stage the estimation of the symbol $\mathbf{s}_m$ can be carried out by using Eq. 15 as the maximum-likelihood function, and the MAP estimate can be expressed as

$$\begin{aligned}\hat{\mathbf{s}} &= \arg\max_{\mathbf{s}_m\in\mathcal{S}}[\mathrm{lr}(\mathbf{s}_m|\mathbf{r})] \\ &= \arg\min_{\mathbf{s}_m\in\mathcal{S}}\|\mathbf{r}-\mathbf{H}\mathbf{s}_m\|^2,\end{aligned} \tag{16}$$

by substituting Eq. 15 into the first equation of Eq. 16. The legitimate constellation symbol $\mathbf{s}_m$ having the smallest distance from the received symbol $\mathbf{r}$ is chosen as the MAP detection result $\hat{\mathbf{s}}$. Finally, the decoded symbol $\hat{\mathbf{s}}$ is mapped to the bits $\hat{\mathbf{b}}$.

## III. Hierarchical Colour-Shift Keying

Based on the standard $M$-CSK regime of [5], we created a variant of the traditional scheme. More specifically, in this section, we will describe our hierarchical CSK (HCSK) modulation schemes as well as their detection methods. Similar to the traditional $M$-CSK modulation scheme, we will rely on the acronym $M$-HCSK using $M$ as the total number of signal points in the symbol set $S$.

### A. The M-HCSK Constellation

*1) Constellation Forming:*

As stated in Section II-A, there are $N_b = \log_2 M$ bits in each M-HCSK symbol. Let us denote these bits by $\mathbf{b}_s$. Since the symbol points in the basic 4-CSK constellation of the can be represented by 2 bits, we partition $\mathbf{b}_s$ by ensuring that every 2 bits correspond to a new layer. Therefore we have $\mathbf{b}_s = \left\{\mathbf{b}_{L_0}, \mathbf{b}_{L_1}, \ldots, \mathbf{b}_{L_{N_L}}\right\}$, where $N_L = N_b/2$ is the total number of layers in each symbol and $\mathbf{b}_{L_l}$, $l \in \{0, 1, \ldots, N_L - 1\}$ represents the 2 bits that correspond to the $l$-th layer. For example, a 16-HCSK symbol $\mathbf{b}_s = b_0b_1b_2b_3$ contains 4 bits per symbol in $N_L = 2$ layers, where $b_0b_1$ are assigned to $L_0$ and $b_2b_3$ are assigned to $L_1$.

Given the symbol constellation of $N_L$-layer M-HCSK and the symbol constellation of the simple 4-CSK, we can readily obtain the symbol constellation of a $(N_L + 1)$-layer 4M-HCSK. Let us now describe the details of the generation method below.

Firstly, given the three vertices $\mathbf{v}_i$, $\mathbf{v}_j$ and $\mathbf{v}_k$ of a triangular CSK constellation plane, the centroid $\mathbf{c}$ of the triangle can be readily obtained according to:

$$\mathbf{c} = \frac{(\mathbf{v}_i + \mathbf{v}_j + \mathbf{v}_k)}{3}. \tag{17}$$

Furthermore, we define the basic vectors (BVs) as the three vectors that have the centroid as the initial point and the three vertices as their individual terminal points, which is formulated as

$$\mathbf{d}_p = \mathbf{v}_p - \mathbf{c}, \tag{18}$$

where we have $p \in \{i, j, k\}$.

Let us now study the $(N_L + 1)$-layer (4M)-HCSK constellation of Fig. 9. The construction process of (4M)-HCSK can be viewed as replacing the points in a standard 4-CSK constellation with the scaled-down versions of the $N_L$-layer M-HCSK constellation, which may also be rotated or flipped. The 2-bit 4-CSK symbols $\mathbf{b}_{s-(4-CSK)}$ , as the new $\mathbf{b}_{L_0}$, are then concatenated as a prefix of their corresponding scaled down M-HCSK symbols $\mathbf{b}_{s-(M-HCSK)}$ , as the new $\mathbf{b}_{L_1 \sim L_{N_L-1}}$, in order to form the new symbol $\mathbf{b}_{s-\{(4M)-HCSK\}}$.

Let us now focus our attention on the (4M)-HCSK constellation, where the three vertices of the triangular constellation area are $\mathbf{v}_p$, $p \in \{i, j, k\}$. Since the layers above $l = 0$ are contained in each of the 4 separate sub-areas, we index these sub-areas by $h$, $h \in \{0, 1, 2, 3\}$. Therefore we will use $\mathbf{v}_{p,h}$, $p \in \{i, j, k\}$ to represent the vertices of each of the 4 areas of layer $l = 1$, where the corresponding BVs are denoted by $\mathbf{d}_{p,h}$ and the centroids by $\mathbf{c}_h$. Since the constellation of each sub-area is transformed from the constellation of the $N_L$-layer M-HCSK, their vertices $\mathbf{v}_{p,h}$ will coincide with the vertices $\mathbf{v}_p$ of the M-HCSK constellation having the same $p$, so that the specific sub-area will inherit both the relative location of the constellation points and the specific bit-to-symbol mapping of M-HCSK, once the vertices have been located. Consider the mapping in Fig. 9a as an example. When $M = 4$, two 4-CSK constellations are used to form the 16-HCSK constellation, where the symbols of a 4-CSK constellation are used as Layer 0, while the symbols of the other one are used as Layer 1. We proceed by first replacing $V_i$ in the constellation representing Layer 0 at the bottom-right corner of Fig. 9a by the constellation representing Layer 1 at the top-right of Fig. 9a, forming sub-area $h = 1$. In the resultant framework of the 16-HCSK constellation seen at the left of Fig. 9a, the vertices of sub-area $h = 1$ have been determined as $\mathbf{v}_{i,1}$, $\mathbf{v}_{j,1}$ and $\mathbf{v}_{k,1}$. Therefore we obtain the location of the constellation points within the sub-area associated with $h = 1$ by appropriately overlapping $\mathbf{v}_{i,1}$, $\mathbf{v}_{j,1}$ and $\mathbf{v}_{k,1}$ with $\mathbf{v}_i$, $\mathbf{v}_j$ and $\mathbf{v}_k$ of the scaled-down version of the constellation at the top-right of Fig. 9a. Since sub-area $h = 1$ is generated by replacing $\mathbf{v}_i$ of the constellation at the bottom-right of Fig. 9a, the newly formed constellation points in sub-area $h = 1$ of the 16-HCSK constellation will obey the new bit-mapping by prefixing '00' to their original bit-mapping.

*2) Symbol Mapping:* However, to locate $\mathbf{v}_{p,h}$, we first have to decide its relative location with respect to the vertex $\mathbf{v}_p$

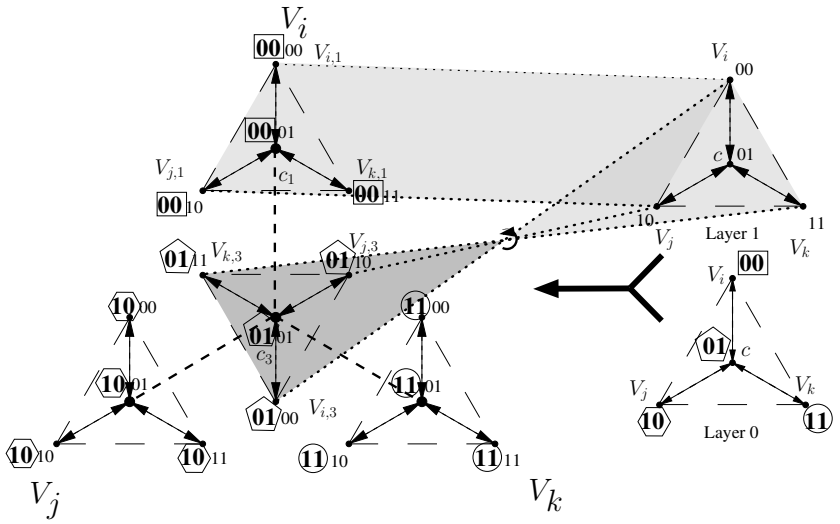


(a) Type I

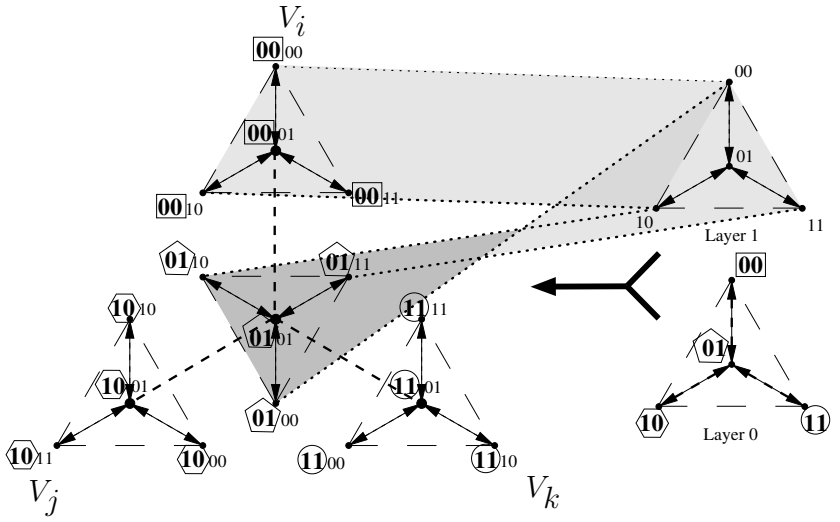


(b) Type II

Figure 9: Generation of the 16-HCSK modulation constellation using the constellation of a basic 4-CSK, following the Type I or Type II design rules.

of (4M)-HCSK. Below, we will proceed by considering this problem in two different ways.

Although having different arrangements for the 4 sub-areas is possible, we can set up some basic rules:

- In order to replace the 4 constellation points of 4-CSK, the position of the $h$-th symbol of 4-CSK must be covered by the $h$-th sub-area of (4M)-HCSK in the replaced constellation. For instance, in Fig. 9a the first symbol $\mathbf{v}_i$ of 4-CSK is covered by sub-area $h = 1$ of the 16-HCSK constellation generated.
- Each vertex $\mathbf{v}_p$ of (4M)-HCSK also constitutes one of the vertices in a certain sub-area. For example, in Fig. 9a the symbol $\mathbf{v}_i$ of the 16-HCSK constellation generated is also the vertex $\mathbf{v}_{i,1}$ of the sub-area $h = 1$.
- The centroid $\mathbf{c}$ of (4M)-HCSK also constitutes the centroid $\mathbf{c}_3$ of the sub-area associated with $h = 3$.
- Each side of the triangular sub-areas must be parallel to the sides of the entire area of (4M)-HCSK constellation, so that the sub-areas are also proportional to the entire area, having a scaling factor of $\alpha$. For example, the sides of the 16-HCSK constellation generated in Fig. 9a are parallel to or partially coincide with the corresponding sides of sub-area $h = 1$.

According to the above rules, we implemented a pair of designs, namely the Type I and II designs of Table. VII. More specifically, the mapping of the sub-area vertices and BVs are specified at certain key constellation points, according to the specifications of Table VIIa, while the rest of the points obey

$$\mathbf{v}_{p,h} = \mathbf{c}_h + \mathbf{d}_{p,h} \tag{19}$$

for $h = 0, 1, 2$ and

$$\mathbf{v}_{p,h} = \mathbf{c}_h - \mathbf{d}_{p,h} \tag{20}$$

specially for $h = 3$. Hence the relationship of $\mathbf{d}_{p,h}$ to the BVs of (4M)-HCSK has now been defined. Finally, we will define

| Vertices | Type I | Type II |
|---|---|---|
| $\mathbf{v}_i$ | $\mathbf{v}_{i,0}$ | $\mathbf{v}_{i,0}$ |
| $\mathbf{v}_j$ | $\mathbf{v}_{j,1}$ | $\mathbf{v}_{i,1}$ |
| $\mathbf{v}_k$ | $\mathbf{v}_{k,2}$ | $\mathbf{v}_{i,2}$ |
| $\mathbf{c}_0$ | $\mathbf{c}_3$ | $\mathbf{c}_3$ |

(a) Mapping of the sub-area vertices and centroids

| BVs of (4M)-HCSK | Type I | Type II |
|---|---|---|
| $\alpha\mathbf{d}_i$ | $\mathbf{d}_{i,0\sim3}$ | $\mathbf{d}_{i,0}$, $\mathbf{d}_{j,1}$, $\mathbf{d}_{k,2}$, $\mathbf{d}_{i,3}$ |
| $\alpha\mathbf{d}_j$ | $\mathbf{d}_{j,0\sim3}$ | $\mathbf{d}_{j,0}$, $\mathbf{d}_{k,1}$, $\mathbf{d}_{i,2}$, $\mathbf{d}_{k,3}$ |
| $\alpha\mathbf{d}_k$ | $\mathbf{d}_{k,0\sim3}$ | $\mathbf{d}_{k,0}$, $\mathbf{d}_{i,1}$, $\mathbf{d}_{j,2}$, $\mathbf{d}_{j,3}$ |

(b) Mapping of the sub-area BVs

Table VII: Parameters of the Type I and II constellation designs showing the specific mapping of the sub-area vertices and BVs to those of (4M)-HCSK's.

the scaling factor $\alpha$ by

$$\begin{aligned}\alpha &= \|\mathbf{d}_{p,h}\| / \|\mathbf{d}_p\| \\ &= \frac{\delta_0\left(\sqrt{M}-2\right)}{2\left(\sqrt{M}-1\right)},\end{aligned} \tag{21}$$

so that when $\delta_0 = 1$ in Eq. (21), the minimum Euclidean distance amongst the vertices $\mathbf{v}_{p,h}$ of different sub-areas also equals $\|\mathbf{d}_{p,h}\|$. In fact, the locations of the 16-HCSK constellation points associated with $\delta_0 = 1$ coincide with those of the standard 16-CSK of [5]. The scaling factor obeys $0 < \alpha < 1/2$, therefore we have $0 < \delta_0 < 1 + 1/\left(\sqrt{M}-2\right)$. Let us now define $\delta_l$, which is the value of $\delta_0$ used for describing the scaling factor $\alpha$ of Eq. (21), when generating the constellation of Layer $l$.

*3) Euclidean Distance:* Let us now investigate the Euclidean distance between the symbol points. Considering the M-HCSK constellation for example, let us partition the constellation points into 4 groups using the definition of the sub-areas. Given $\delta_l = 1$ for $l > 0$, the minimum Euclidean distance among the symbols within each group can be expressed as

$$dist_{ig} = \frac{\delta_0}{\sqrt{M}-1}\min\|\mathbf{d}_p\|. \tag{22}$$

By contrast, the minimum Euclidean distance between the different symbol groups is

$$dist_{ag} = \left(1 - \frac{\sqrt{M}-2}{\sqrt{M}-1}\delta_0\right)\min\|\mathbf{d}_p\|. \tag{23}$$

For example, when assuming $\delta_0 = 1$ for the case of the 16-HCSK constellation shown in Fig. 9a, we have $dist_{ig} = dist_{ag} = \|\mathbf{d}_i\|/3$, which implies that the minimum Euclidean distances are the same both within and between group(s). From Eq. (22) and Eq. (23) we find that $dist_{ag}$ decreases as $\delta_0$ increases, which results in an increased SER for layer $l = 0$. At the same time, $dist_{ig}$ increases as $\delta_0$ increases, which suggests having a reduced SER for the higher layers associated with $l > 0$, despite the presence of cross-layer interferences. For example, when assuming $\delta_0 = 1.2$ in Fig. 9a, we have $dist_{ig} > \|\mathbf{d}_i\|/3$, which means that the symbol '0010' is less likely to be confused with '0001', when contaminated by channel distortions. In this case the last two bits of the symbol belonging to Layer 1 may appear to be better protected. However, at the same time we have $dist_{ag} < \|\mathbf{d}_i\|/3$, which means that symbol '0010' in sub-area $h = 0$ can easily be confused with '0111' in sub-area $h = 3$. In this case both the first and last two bits corresponding to 2 layers are more error-prone. However, looking at the differences between the type I and II symbol mappings in Table VII, we find that the neighbouring symbols between each two groups of symbols have the same bit-mapping for $l > 0$, which is aimed at reducing the SER degradation of the higher layers owing to the increased cross-layer interferences encountered upon increasing $\delta_0$. For example, when assuming $\delta_0 = 1.2$ in Fig. 9b, we still have $dist_{ag} < \|\mathbf{d}_i\|/3$, which means that symbol '0010' in sub-area $h = 0$ can easily be confused with '0110' in sub-area $h = 3$. In this case only the first two bits corresponding to Layer 0 are more error-prone, while the last two bits corresponding to Layer 1 are less prone to errors, even if the symbol is misjudged, because these two nearby symbols are the same for the last two bits.

### *B. Layer-by-layer Demodulation of M-HCSK*

As stated in Section III-A, each M-HCSK symbol $\mathbf{s}_m$ can be represented by $\mathbf{b}_s = \left\{\mathbf{b}_{L_0}, \mathbf{b}_{L_1}, \ldots, \mathbf{b}_{L_{N_L-1}}\right\}$, where $\mathbf{b}_{L_l}$, $l \in \{0, 1, \ldots N_L - 1\}$, corresponds to the $l$-th layer. Since $\mathbf{b}_{L_l}$ is a 2-bit symbol, it has 4 possible values, namely '00', '01', '10' and '11'. Let us denote these 4 values by $\mathbf{b}_{h_l}$, where $h_l \in \{0, 1, 2, 3\}$. Therefore, the layer-by-layer demodulation of M-HCSK can be carried out by firstly obtaining the *a posteriori* probability of $\mathbf{b}_{h_l}$s, formulated as:

$$\Pr\left(\mathbf{b}_{h_l}|\,\mathbf{r}\right) = \sum_{\mathbf{b}_s \in \left\{\mathbf{b}_{s'}|\mathbf{b}_{L_l}=\mathbf{b}_{h_l}\right\}} \Pr\left(\mathbf{b}_s|\,\mathbf{r}\right), \tag{24}$$

where $\Pr\left(\mathbf{b}_s|\,\mathbf{r}\right)$ was expressed in Eq. (14) and Eq. (15). Therefore the decision on $\mathbf{b}_{L_l}$ can be formulated as:

$$\hat{h}_l = \underset{h\in\{0,1,2,3\}}{\arg\max}\ \Pr\left(\mathbf{b}_{h_l}|\,\mathbf{r}\right) \tag{25}$$

and

$$\hat{\mathbf{b}}_{L_l} = \mathbf{b}_{\hat{h}_l}. \tag{26}$$

However, the procedure represented by Eq. 24 imposes a high computational complexity, which requires the calculation and summing of $4^{N_L-1}$ different $\Pr\left(\mathbf{b}_s|\,\mathbf{r}\right)$s. In order to reduce the complexity imposed, we may simplify Eq. (24) by replacing the *a posteriori* probabilities of the $\mathbf{b}_{L_l}$ represented symbol sub-groups with that of the centroid of the corresponding sub-area of the constellation, yielding:

$$\Pr\left(\mathbf{b}_{h_l}|\,\mathbf{r}\right) = \sum_{h_l=h}\Pr\left(\left.\underbrace{\mathbf{c}_{h_0,h_1,\ldots h_l}}_{l+1}\right|\mathbf{r}\right), \tag{27}$$

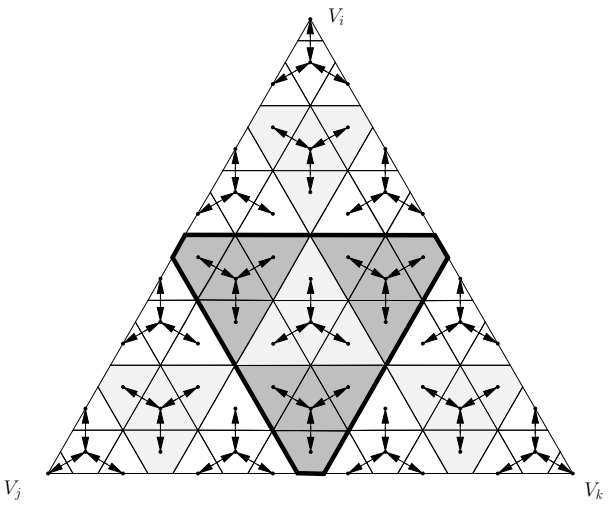


Figure 10: Colour constellation of 64-HCSK

where $\mathbf{c}_{h_0,h_1,\ldots h_l}$ stands for the centroid of the triangular sub-area constituted by the constellation points of the symbols $\mathbf{b}_s \in \{\mathbf{b}_{s'} | \mathbf{b}_{L_0} = \mathbf{b}_{h_0}, \mathbf{b}_{L_1} = \mathbf{b}_{h_1}, \ldots, \mathbf{b}_{L_l} = \mathbf{b}_{h_l}\}$. Therefore in Eq. (27) the *a posteriori* probabilities $\Pr\left(\underbrace{\mathbf{c}_{h_0,h_1,\ldots h_l}}_{l+1} \middle| \mathbf{r}\right)$ are summed over different values of $h_0, h_1, \ldots h_{l-1}$ with a fixed $h_l$, to get the result for $\Pr(\mathbf{b}_{h_l} | \mathbf{r})$. By replacing the $4^{N_L-l-1}$ symbols in a sub-area with their associated centroid, Eq. (27) reduces the complexity to $4^l$ instead of $4^{N_L-1}$.

If no FEC is used and hence only detection decisions are required for generating the modulation output, the previous process of Eq. (24) and Eq. (25) can be further simplified by making the decisions in a layer-by-layer manner, yielding:

$$\hat{h}_l = \underset{h\in\{0,1,2,3\}}{\arg\min} \left\| \mathbf{r} - \mathbf{H}\mathbf{c}_{\underbrace{\hat{h}_0, \hat{h}_1, \ldots, \hat{h}_{l-1}, h}_{l+1}} \right\|^2 . \quad (28)$$

Namely, by using Eq. (28), we first make decisions of $\hat{h}_0$ associated with layer $l = 0$ and work our way up based on the decisions made for the previous layers. Therefore the estimation $\hat{h}_0, \hat{h}_1, \ldots, \hat{h}_{l-1}$ of $h_0, h_1, \ldots h_{l-1}$ will be attained in the above order, and the next decision for $h_l$ can be readily obtained by applying Eq. (28). In this way only four Euclidean distance computations are required for a decision.

By using the reduced complexity demodulation method of Eq. (28), we obtained the frame error ratio (FER) versus the values of $\delta_l$ using either the 16-HCSK or 64-HCSK for a transmission frame length of 1200 bits, as shown in Fig. 11. The construction of 64-HCSK is carried out using the method of Section III-A, which results in the constellation shown in Fig. 10. By observing Fig. 11, we can clearly see the differences between the Type I and Type II constellation designs of Table VII in terms of the FERs of each decoded M-HCSK layer. For example, by comparing Fig. 11a and 11c, we can see that as the parameter $\delta_0$ defined in Eq. (21) for 16-HCSK increases, the FER of Layer 0 increases for both the Type I and II regimes of Table VII. However, when the FER of Layer 1 is considered, for Type I it first decreases until around $\delta_0 = 1$, then it is increased again, while it is reduced all along as $\delta_0$ increases for Type I. The reason behind this is that as $\delta_0$ increases, the cross-layer interferences become more significant, as described in Section III-A. While the cross-layer interferences result directly in an increase of the FER of Layer 1 in the Type I constellation, the mapping of the Type II constellation prevents this, because the adjacent Layer 1 symbols belong to different Layer 0 symbol groups having the same bit mapping in Layer 1, as seen in the constellation of Fig. 9b. Similar properties can be observed for the FERs of 64-HCSK in Fig. 11b and Fig. 11d. Explicitly, observe that the Type II constellation provides a wider range of FERs for the higher layers upon varying $\delta_l$ according to Fig. 11, therefore it is more promising in terms of reducing the effect of cross-layer interferences, hence providing a high grade of flexibility in terms of system configuration and optimization.

## IV. Video Transmission System

In this section, we will introduce a video streaming system relying on our M-HCSK modulation scheme and a RSC FEC code, as shown Fig. 12.

### A. Source Coding

As shown in Fig. 12, the original video sequence is firstly encoded into a scalable video stream by invoking the SVC extension of H.264 [41]. The compressed video stream consists of $N_v$ layers, namely of $Lv_0$, $Lv_1$,... $Lv_n$, $n \in \{0, 1, \ldots, N_v - 1\}$, with the dependency of $Lv_0 \Leftarrow Lv_1 \Leftarrow \ldots \Leftarrow Lv_n$, where each item on the right of the $\Leftarrow$ symbol depends on all the items to the left of it. To utilize the $n$-th layer for successful decoding, the decoder has to invoke the information from all the previous $n$ layers ranging from $Lv_0$ to $Lv_{n-1}$. The different layers $Lv_n$ of the compressed video stream have different number of bits. Let us denote the length of the $n$-th layer by $\ell v_n$. In order to make the video layers robust to transmission errors, their multiplexing has to be carefully designed.

### B. Channel Coding and Video-to-M-HCSK Mapping

Two specific types of FEC codes have been adopted in the IEEE 802.15 standard [5] for VLC, namely a RS code and a convolutional code (CC). In this treatise we employed a RSC code, which is similar to the CC used in the standard. As shown in Fig. 13, the classic multiplexing would feed the compressed video stream to the FEC encoder and modulator sequentially. However, the system will not benefit from the layered structure of the video stream and of the M-HCSK modulator for this conventional equal error protection (EEP) scheme. In order to exploit the above-mentioned layered structure, we conceived the beneficial video bit to M-HCSK mapping scheme of Fig. 13b.

Hence observe in Fig. 13b that according to the number of M-HCSK layers, $N_L$ buffers are used for storing the compressed output of the SVC video encoder. These buffers

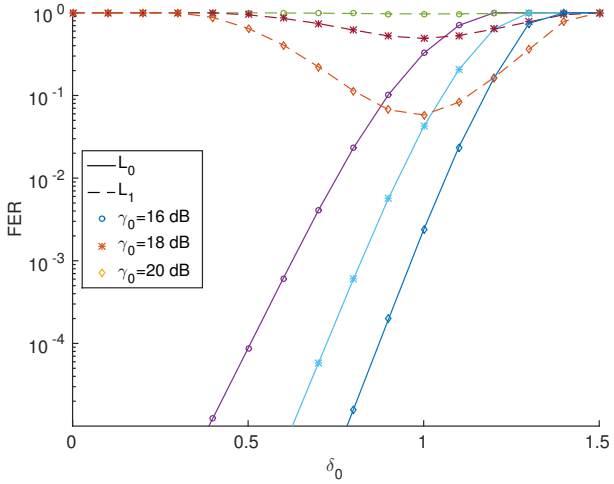


(a) FER vs. $\delta_0$ using Type I 16-HCSK, for various optical SNRs

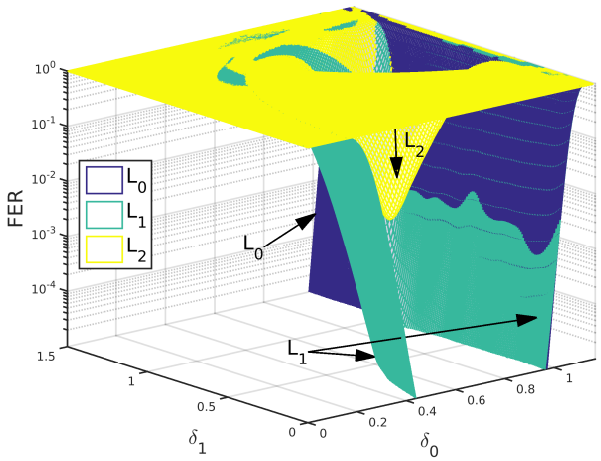


(b) FER vs. $\delta_0$ and $\delta_1$ using Type I 64-HCSK, for an optical SNR of $\gamma_0 = 28dB$

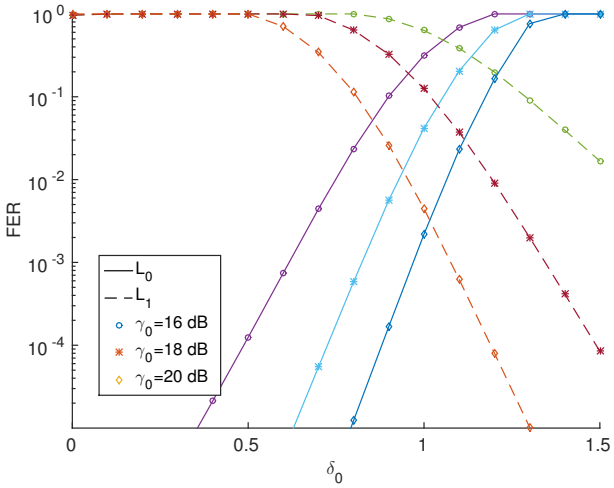


(c) FER vs. $\delta_0$ using Type II 16-HCSK, for various optical SNRs

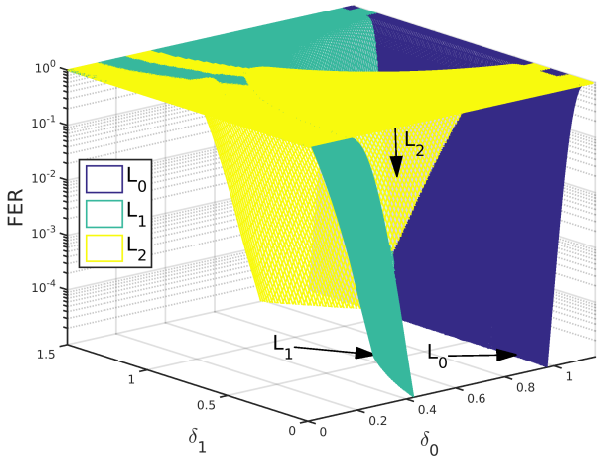


(d) FER vs. $\delta_0$ and $\delta_1$ using Type II 64-HCSK, for an optical SNR of $\gamma_0 = 28dB$

Figure 11: FER vs. $\delta_l$ of Type I and II 16/64-HCSK modulation, using a frame length of 1200 bits.

are denoted as $Bf_l$, $l \in \{0, \ldots, N_L - 1\}$, ranging from top to bottom. Each layer has the same length of

$$\ell_{Bf} = \left\lceil \frac{1}{N_L} \sum_{n \in \{0,1,\ldots,N_v-1\}} \ell v_n \right\rceil \tag{29}$$

bits. The $N_v$ video layers are written into those buffers sequentially, commencing from the BL and gradually proceeding with the ELs having higher levels of dependency. When the $n$-th buffer is filled up, the mapping process will continue from the beginning of the $(n+1)$-st buffer. When the mapping of all the video layers is finished, the remaining storage space left in the buffer will be filled by bits of '0'.

In the channel coding process, $N_L$ FEC encoders read simultaneously from the $N_L$ data buffers, each taking $\ell_F$ bits at a time. The FEC coded bits of the $n$-th data buffer will be used as the input of the $n$-th layer of the M-HCSK modulator. Those $N_L$ FEC encoded data frames are mapped to a single M-HCSK frame. By adopting this multiplexing scheme, we have ensured that the $N_v$ number of video layers having different bit-lengths are mapped to $N_L$ streams having the same lengths. More importantly, we ensure that the video frames corresponding to a single M-HCSK frame are strictly sorted according to their importances, bearing in mind the level of dependencies they have. The FEC frames corresponding to the BL will always occupy the highest-integrity layer of the M-HCSK, while the ELs are mapped to higher layers.

Fig. 13b shows an example of the multiplexing results, where we have $N_v = N_L = 3$. Consequently, the M-HCSK frames have three types. Specifically, let us denote the $t$-th M-HCSK frame by $F_t$. Then $F_0$ and $F_1$ has the type $Lv_0 - Lv_1 - Lv_2$, $F_2$ has the type $Lv_0 - Lv_2 - Lv_2$, while the rest of the frames has the type $Lv_1 - Lv_2 - Lv_2$. Generally, let us denote the total number of M-HCSK frame types by $N_T$.

### C. Modulation Optimization

Given the transmission scheme of Fig. 12 described in Section IV-A and IV-B, we aim for optimizing the modem parameters for to ensuring that the system achieves its best performance. More specifically, the distortion of the video reconstructed at the receiver end should be minimized.

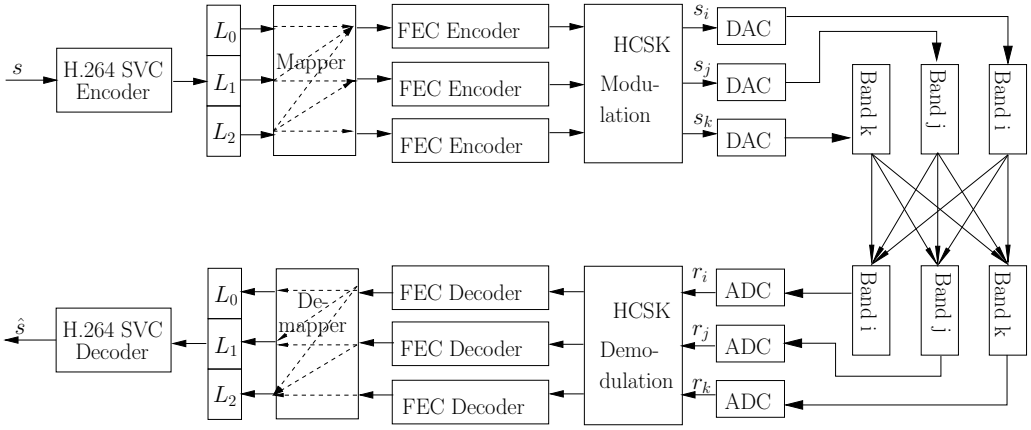


Figure 12: Transceiver architecture of the M-HCSK-RSC scheme conceived for scalable video transmission over VLC channels.

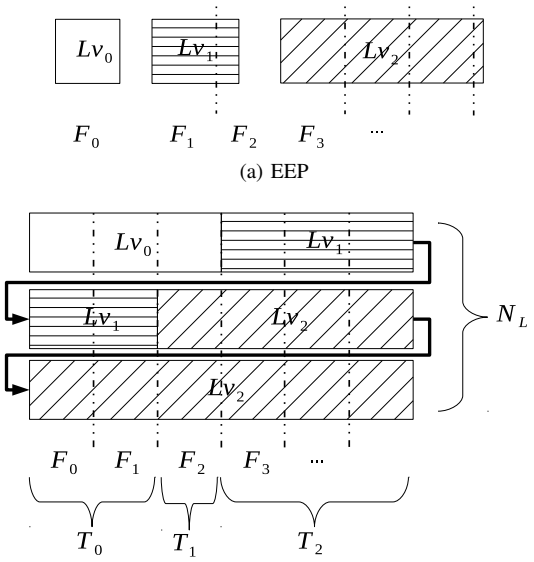


(a) EEP

(b) UEP

Figure 13: EEP and UEP versions of the video-to-M-HCSK for scalable video transmission.

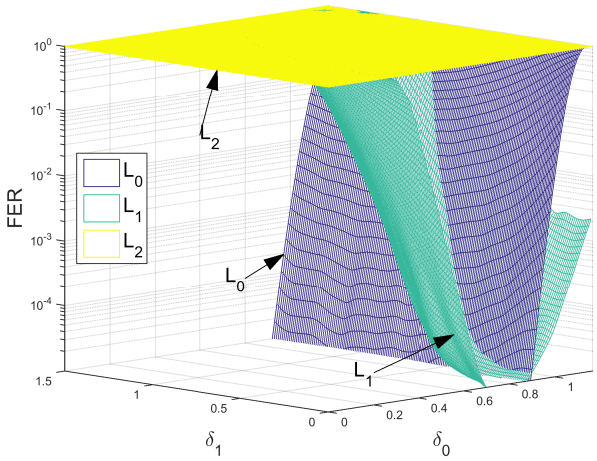


(a) FER vs. $\delta_l$s using Type I 64-HCSK

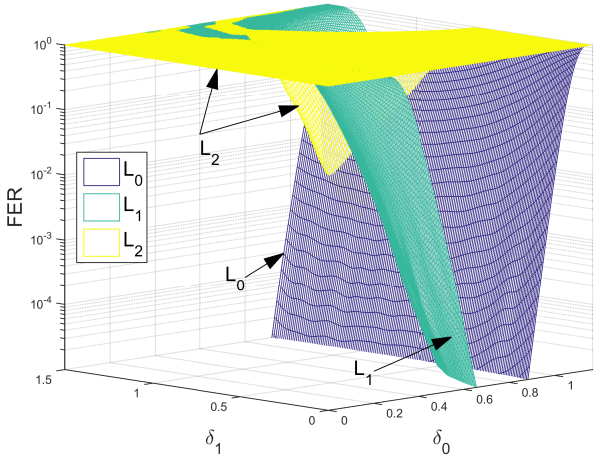


(b) FER vs. $\delta_l$s using Type II 64-HCSK

Figure 14: FER vs. $\delta_0$ and $\delta_1$ of the M-HCSK-RSC transmission systems of Fig. 12 using Type I or II 64-HCSK modulation at the optical SNR of $\gamma_0 = 20\,dB$. A frame length of 1200 bits is used.

In order to estimate the video distortion, we require the conditional FER $p_n$ associated with each video layer's FER and its distortion $\epsilon_n$. The conditional FER $p_n$ is defined as the FER of the $n$-th video layer, given that all the bit streams gleaned from the previous layers having an index ranging from 0 to $n-1$ are intact. The distortion $\epsilon_n$ imposed by the loss of layer $n$ can be obtained by the so-called off-line removal-decoding test, which was advocated in [114] and [115]. Before the commencement of transmissions, $\epsilon_n$ is measured by the process based on the PSNRs of the reconstructed video with the bit stream of the $n$-th video layer removed, and of the one relying on the intact bit stream of the $n$-th video layer.

Firstly, let us define another conditional FER $p_{t,l}$, which refers to the FER of the $l$-th layer of the $t$-th M-HCSK frame after RSC decoding, provided that the previous $l$ layers in the $t$-th M-HCSK frame have been successfully recovered. The FER $p_{t,l}$ can be formulated by introducing the function $f_l(.)$, which can be expressed as

$$\begin{aligned} p_{t,l} &= f_l\left(\gamma_o, \ell_F, \delta_{t,0}, ..., \delta_{t,N_L-2}\right) \\ &= 1 - \left[1 - \mathcal{T}\left[\gamma_o, \delta_{t,0}, ..., \delta_{t,N_L-2}\right]\right]^{\ell_F/\ell}. \end{aligned} \tag{30}$$

As shown in Eq. 30, the knowledge of the optical SNR $\gamma_o$, the length $\ell_F$ of each M-HCSK frame and of the M-HCSK parameters $\delta_{t,l}$, $l \in \{0, 1, \ldots, N_L - 2\}$ corresponding to the $t$-th M-HCSK frame are all required for to estimating $p_{t,l}$. At the right hand side of Eq. 30, a pre-stored look-up table (LUT) $\mathcal{T}(\cdot)$ is used for obtaining the FER assuming a fixed transmission frame-length of $\ell$ bits. More specifically, the LUT $\mathcal{T}(\cdot)$ has $N_L$ entries corresponding to the specific FER evaluated as a function of both the SNR and of the M-HCSK parameters.

Given the expression of $p_{t,l}$ in Eq. 30, we can now readily obtain the conditional FER $p_n$ as

$$p_n = 1 - \prod_{\{t,l|\mathfrak{m}(t,l)=n\}} (1 - p_{t,l}), \tag{31}$$

which exploits the following assumptions. The mapping function $\mathfrak{m}(t,l)$ of Eq. (31) returns the index of the video layer associated with the $l$-th layer of the $t$-th M-HCSK frame. Therefore the calculation of $p_n$ in Eq. (31) relies on all the parts of the $n$-th video layer that are distributed across the different M-HCSK frames or layers.

Having obtained $\epsilon_n$ and $p_n$, we can now readily estimate the expected decoded video distortion in analogy with the approaches in [116]–[124], which are the contributions on adaptive or unequal-protected streaming of layered media (layered video or layered image) and have similar video distortion models according to the package-losses. However, they have subtle differences depending on the specific experimental methods they adopted for obtaining the related parameters. Several authors [116]–[122], tackle this issue by quantifying the video distortions in the absence of certain packets. By contrast, some works opt for measuring the video distortion reduction in the presence of certain packets [123], [124]. Therefore there are some minor but non-negligible differences in their distortion-estimation expressions. We will follow the first category in the distortion estimation in this treatise. Given the FER expression of $p_n$, the expected decoded video distortion at the receiver can be formulated as:

$$\begin{aligned} & e(\gamma_o, \delta_{0,0}, \ldots, \delta_{t,l}, \ldots) \\ & = \mathbf{D}_0 + \mathbf{D}_1 + \ldots + \mathbf{D}_{N_V-1} \\ & = p_0 \cdot \epsilon_0 + [1 - p_0] \cdot p_1 \cdot \epsilon_1 + \ldots \\ & = \sum_{n=0}^{N_V-1} \epsilon_n \cdot p_n \cdot \prod_{j=0}^{n-1} [1 - p_j], \end{aligned} \tag{32}$$

where $p_n \cdot \prod_{j=0}^{n-1}[1-p_j]$ represents the probability of the video layer $n$ being corrupted and $\mathbf{D}_n = \epsilon_n p_n \cdot \prod_{j=0}^{n-1}[1-p_j]$ represents the corresponding video distortion introduced, while the layers $0 \sim n-1$ have been successfully received. Observe in Eq. 32 that the video distortion estimation requires the value of $\delta_{t,l}$, which represents $\delta_l$ adopted at time slot $t$, for $l \in \{0, 1, \ldots, N_L - 2\}$ and $t \in \{0, 1, \ldots, T-1\}$. Hence there are as many as $(N_L - 1) \cdot T$ $\delta_{t,l}$ values. For instance, 16-HCSK needs $T$ $\delta_{t,l}$ values, while 64-HCSK requires $2T$ $\delta_{t,l}$ values. However, in practice there are only a few different types of M-HCSK frames. Assuming that there are $K$ different M-HCSK frames, we have $K \leq N_v < T$. For instance, if a video stream containing three layers is transmitted over a larger number of time slots, there are at most three different types of M-HCSK frames. Consequently, we can reduce the number of $\delta_{t,l}$ values to $K \cdot T$. Let us furthermore denote these different types of M-HCSK frames by $T_k$, where we have $k \in \{0, 1, ..., K-1\}$, as shown in Fig. 13b.

| | Soccer | Ice | Crew |
|---|---|---|---|
| Representation | YUV 4:2:0 | | |
| Format | 4CIF | | |
| Bits Per Pixel in Each Y, U, V Channel | 8 | | |
| FPS | 60 | | |
| Number of Frames | 60 | | |
| Video Codec | SVC-H.264 | | |
| Codec Version | JSVM 9.19.14 | | |
| GOP | 15 | | |
| Scalability | MGS | | |
| Bitrate | 19.30 Mbps | 6.01 Mbps | 11.50 Mbps |
| Error-Free PSNR | 42.25 dB | 44.56 dB | 42.89 dB |
| Error Concealment | Frame-Copy | | |

Table VIII: The video parameters

Finally, as stated before, we want to optimize the system by minimizing the distortion of the decoded video. Hence the final decision concerning the M-HCSK parameters may be formulated as:

$$\mathbf{D}(\gamma_o) = \underset{0<\delta_{k,l}<\delta_{max,l}}{\arg} \min \{e(\delta_{0,0}, \ldots, \delta_{k,l}, \ldots)\}, \tag{33}$$

where $k \in \{0, \ldots, K-1\}$.

The optimization of Eq. (33) can be readily handled by optimization tools, such as the function *fmincon* in MATLAB. To solve the problem of Eq. (33) as a function of the parameters $\delta_{k,l}$s ($k \in \{0, \ldots, K-1\}$, $l \in \{0, 1, \ldots, N_L - 2\}$) under the constraint of $0 < \delta_{k,l} < \delta_{max,l}$, Eq. (33) is forwarded to the *fmincon* function of the optimization toolbox in MATLAB. The optimization of the objective function at the values of $\delta_{k,l}$ is carried out using the interior point method of the fmincon function provided in the MATLAB optimization toolkit. The fmincon function begins with the initial values of $\delta_{k,l}$ set to 1, then stops when the first order optimality measure defined as the maximum of the stationarity and complementary slackness Karush–Kuhn–Tucker conditions becomes lower than a specified tolerance [125].

## V. System Performance

In this section, we will quantify the attainable performance gain of our proposed M-HCSK-RSC transmission scheme. Three 4:2:0 YUV format video sequences were chosen for

| Category | Parameters | |
|---|---|---|
| LED bandwidth | Blue | 380 - 478 nm, centre of 429 nm |
| | Yellow | 540 - 588 nm, centre of 564 nm |
| | Red | 726 - 780 nm, centre of 753 nm |
| $R$ | 1 A/W | |
| $T$ | 293 K | |
| $\frac{P_{Daylight}}{P_{Signal}(t)}$ | 11% | |

Table IX: The VLC related parameters used in Section V.

| Category | Regime |
|---|---|
| Constellation Size | 16-HCSK-RSC with 2 layers |
| | 64-HCSK-RSC with 3 layers |
| Constellation Type | Type I |
| | Type II |
| UEP/EEP | EEP |
| | Optimized UEP |

Table X: The regimes with their settings characterized in Section V.

transmissions, namely the Soccer, the Ice and the Crew video clips. These 60-frame sequences are in the $(704 \times 576)$-pixel 4CIF format, and were recorded at 60 FPS.

### A. Layered Video Codec Settings

We use the JSVM H.264/AVC reference video codec (JSVM 9.19.14), which relies on a group of pictures (GOP) duration of 15 frames and the bi-directionally predicted (B) frames are disabled, as we are aiming for a lip-synchronised transmission design with small latency and low complexity [126]. We enabled the Medium Grain Scalability (MGS) [40], [127] feature for encoding the video sequences into three layers with the aid of the standardized video quantization parameters (QP) of 46, 34 and 25, respectively. The average PSNRs achieved by the decoder for the three sequences are 42.25 dB, 44.56 dB and 42.89 dB, respectively.

Based on our configuration of the SVC encoder, each slice is encoded into three layers and each layer is encapsulated into a network abstraction layer unit (NALU) [41]. The NALUs are transmitted sequentially using our proposed system. Should the Cyclic Redundancy Check (CRC) of a certain NALU indicate a decoding failure, these NALUs are discarded. The SVC decoder uses the low-complexity error concealment method of 'previous frame-copying' [128], [129] in order to replace the lost frames. The main video system parameters are listed in Table VIII.

### B. VLC Transmission System Settings

Here we will describe the parameters associated with each of the transmission modules of our proposed M-HCSK-RSC transmission scheme shown in Fig. 12. As the FEC codec, an RSC code having a code-rate of $1/2$ and the generator polynomials of $[10011, 00110]$ is employed in our system of Fig. 12.

As shown in Fig. 4 and 12, our system uses three LED transmitters of different light bands. More specifically, our VLC transceiver consists of Red, Yellow and Blue LED transmitters and their corresponding PDs. The light bands of the LEDs are stipulated in Table IX. According to the IEEE 802.15 standard [5], the data rate of the standard CSK depends on the optical clock rate adopted. For instance, when the optical clock rate of 24 MHz is used, the corresponding 8/16-CSK with half-rate FEC operate at the data-rate of 36 Mbps and 48 Mbps respectively. As our 16-HCSK has the same bits per symbol as 16-CSK while our 64-HCSK has twice the bits per symbol of 8-CSK, they will have the data-rates of 48 Mbps and 72 Mbps respectively, under the same systems settings.

Our VLC transmission model was introduced in Section II-B, with the corresponding parameters listed in Table IX. The channel matrix $\mathbf{H}$ in the transmission model of Eq. (7) is an identity matrix, representing a non-dispersive AWGN channel, with $\mathbf{n}$ being the AWGN having a total power of $\sigma^2 = E_s/\gamma_o$.

In order to characterize the performance of our optimised system, we compare our UEP scheme to the traditional EEP scheme for transmission, as listed in Table X. Furthermore, two types of M-HCSK constellation mapping configurations listed in Section III-A2, namely the Type I and Type II constellation designs were simulated. Finally, two M-HCSK constellation sizes were considered, namely the 16-HCSK with 2 modulation layers and the 64-HCSK with 3 modulation layers.

### C. Calculation of PSNR

In this treatise we are interested in the PSNR of the Y frames of the decoded video. Here we introduce the detailed calculation method of the previously mentioned PSNR, as our video quality metric. Let us commence by stipulating the following assumptions

- $(m \times n)$: the resolution of the luminance frame;
- $I(i,j)$: the original/reference video pixel value at position $(i,j)$ of a specific video frame;
- $K(i,j)$: the reconstructed pixel value at position $(i,j)$ of a specific video frame;

Then the PSNR is calculated as follows

$$\begin{aligned} MSE &= \frac{1}{mn} \sum_{i=0}^{m-1} \sum_{j=0}^{n-1} [I(i,j) - K(i,j)]^2 \\ PSNR_{dB} &= 20 \cdot \log_{10} \frac{\max(I)}{\sqrt{MSE}}. \end{aligned} \tag{34}$$

However, small mean square error (MSE) values may result in infinite PSNR values. Hence the following modified PSNR

calculation is employed

$$\begin{aligned} MSE &= \frac{1}{mn}\sum_{i=0}^{m-1}\sum_{j=0}^{n-1}[I(i,j)-K(i,j)]^2 \\ PSNR_{dB} &= 20\cdot\log_{10}\frac{\max(I)}{\sqrt{MSE'}} \\ MSE' &= \max(1, MSE), \end{aligned} \tag{35}$$

which results in a maximum PSNR value of 48.13 dB. Since we are observing the Y frames, the $PSNR_{dB}$ of each Y frame is averaged over the entire video sequence.

### D. Off-line LUT Generation

As described in Eq. 30 of Section IV-C, the estimation of the FER relies on the LUT $\mathcal{T}(\cdot)$. Here we describe the generation of the LUT $\mathcal{T}(\cdot)$ used in our experiments. As mentioned in Section IV-C, the LUT $\mathcal{T}(\cdot)$ is indexed by two types of parameters, namely the $SNR$, and the $\delta_l$ parameters, where $l \in \{0, 1, \ldots, N_L - 2\}$. To generate the LUT $\mathcal{T}(\cdot)$, we fix the block-length $\ell$ of the FEC and obtain the FER $p(\ell)$ of the component FEC by scanning the practical coding parameter ranges of $SNR$ and $\delta_l$ at certain intervals. Specifically, the $SNR$ is considered over the range of $[8, 26]$ dB, using a step-size of 0.5 dB. The $\delta_l$ values are non-linearly scanned over the range of $\left(0, \frac{\sqrt{M}-1}{\sqrt{M}-2}\right)$, using a step-size of 0.01 over the range of $(0, 0.5]$, and using a step-size of 0.005 over the range of $\left(0.5, \frac{\sqrt{M}-1}{\sqrt{M}-2}\right)$. This will constitute a total number of $n_{\mathcal{T}} = n_{snr} n_r^{N_L-1} = 37 \times \left(50 + \left\lfloor \frac{100\sqrt{M}}{(\sqrt{M}-2)} \right\rfloor\right)^{N_L-1}$ legitimate settings. For the 16-HCSK-RSC system of Table X, we have $N_L = 2$, $M = 16$ and therefore $n_{\mathcal{T}} = 9,250$. On the other hand, we have $N_L = 3$, $M = 64$ for the 16-HCSK-RSC system of Table X and therefore $n_{\mathcal{T}} = 1,239,093$. For each optimized UEP regime, a LUT is needed. By combining all the LUTs $\mathcal{T}(\cdot)$, for $l \in \{0, 1, \ldots, N_L - 1\}$, we have $2N_L$ items per setting. An example can be found in Tab. XI, showing the LUT needed for the Type I 64-HCSK system using our optimized UEP regime. Since each item in the LUTs can be individually stored as floats in 8 bytes, the total size of the LUT for our 16-HCSK-RSC system is 289 KB and that of the 64-HCSK-RSC system is 56.72 MB.

In order to examine our LUT based FER estimation, we depicted the FER vs. simulated optical SNR $\gamma_0$ of 16-HCSK-RSC transmission for different frame lengths in Fig. 15. It can be observed that the estimated FERs using a frame length of 1200 bits closely coincide with the simulated results, therefore our LUT based FER estimation is reliable.

### E. Optimized System Parameters

In order to characterize the PSNR versus optical SNR $\gamma_0$ performance of our proposed optimised UEP M-HCSK-RSC system, we compare them to the traditional EEP M-HCSK-RSC scheme for transmission over an AWGN channel, as listed in Table X. These comparisons are shown in Fig. 16, which were carried out using the above-mentioned three different video sequences, namely the Soccer, the Ice and the Crew sequences, as listed in Table VIII. The previous Type I and Type II M-HCSK constellation designs were simulated, as described in Section III-A.

| Optical SNR($dB$) | $\delta_0$ | $\delta_1$ | $p_0(\ell)$ | $p_1(\ell)$ | $p_2(\ell)$ |
|---|---|---|---|---|---|
| ... | ... | ... | ... | ... | ... |
| 13 | 0.95 | 0.05 | 0.357741 | 0.953467 | 1 |
| 13 | 0.95 | 0.10 | 0.307621 | 0.955615 | 1 |
| 13 | 0.95 | 0.15 | 0.273464 | 0.957082 | 1 |
| 13 | 0.95 | 0.20 | 0.230841 | 0.959333 | 1 |
| 13 | 0.95 | 0.25 | 0.196220 | 0.960815 | 1 |
| 13 | 0.95 | 0.30 | 0.168964 | 0.969287 | 1 |
| 13 | 0.95 | 0.35 | 0.146773 | 0.974093 | 1 |
| ... | ... | ... | ... | ... | ... |

Table XI: Example of the LUT of Type I 64-HCSK.

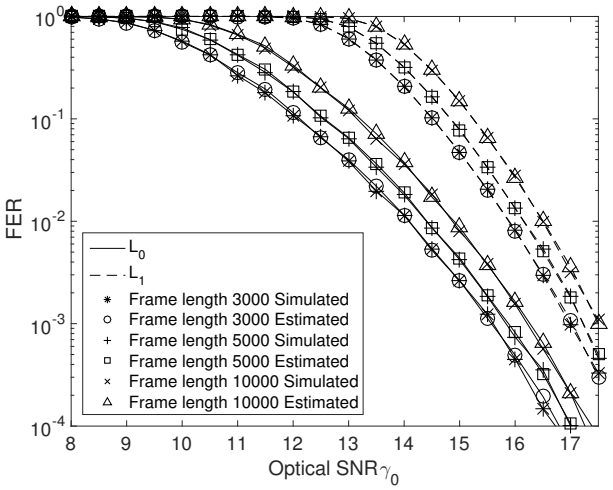


Figure 15: FER vs. simulated optical SNR $\gamma_0$ of 16-HCSK-RSC transmission with different frame lengths. Both simulated and estimated results using a frame length of 1200 bits are shown.

The results recorded for the Soccer sequence with the aid of 16-HCSK are shown in Fig. 16a. We can observe that both UEP schemes relying on the Type I and Type II constellations outperformed their corresponding EEP counterparts. More specifically, when the Type II constellation design of Table VII is adopted, the optimised UEP system outperforms the EEP benchmark and achieves an optical SNR reduction of about $1.4$ $dB$ at a PSNR of 37 $dB$, which correspond to the scenario of receiving all video layers with a high probability. To elaborate a little further, the staircase-shaped nature of these PSNR curves explicitly indicates the number of video layers received flawlessly. Similarly, for the Type I constellation design of Table VII, the optimised UEP system achieves an optical SNR reduction of about $1.1$ $dB$ at a PSNR of 37 $dB$. Additionally, it can be observed that the UEP schemes associated with the Type II HCSK constellation perform significantly better than the Type I HCSK, and an optical SNR reduction of about $1.1$ $dB$ can be achieved at a PSNR of 37 $dB$ by using the former over the latter. This suggests that the system associated with the Type II HCSK constellation design is more capable.

Now that we have inspected the performance of our optimised UEP M-HCSK-RSC system at higher optical SNR

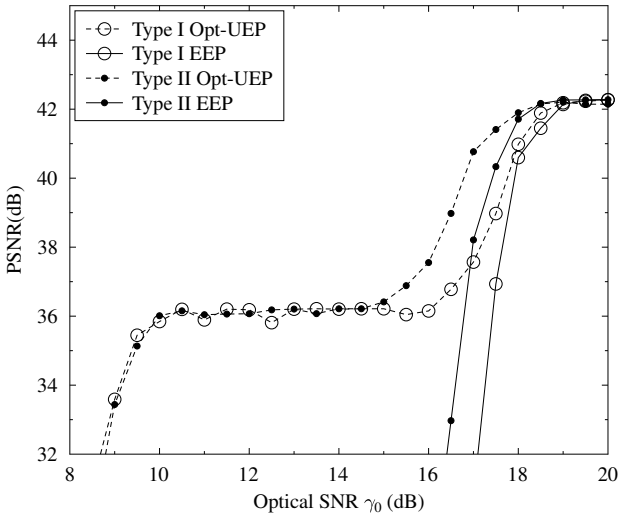


(a) PSNR vs optical SNR $\gamma_0$ for *Soccer* with 16-HCSK-RSC

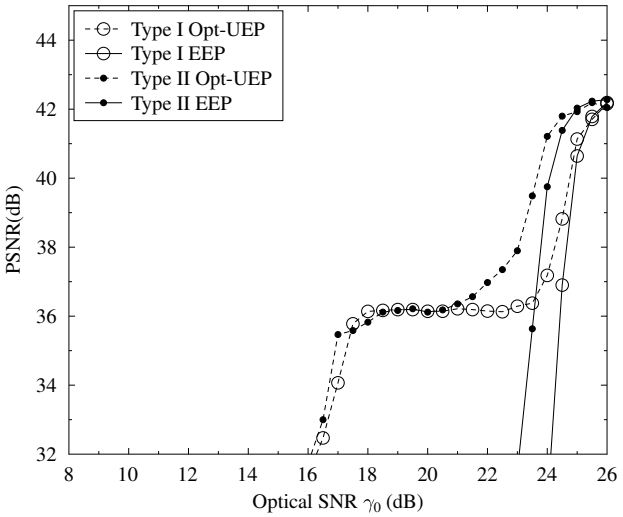


(b) PSNR vs optical SNR $\gamma_0$ for *Soccer* with 64-HCSK-RSC

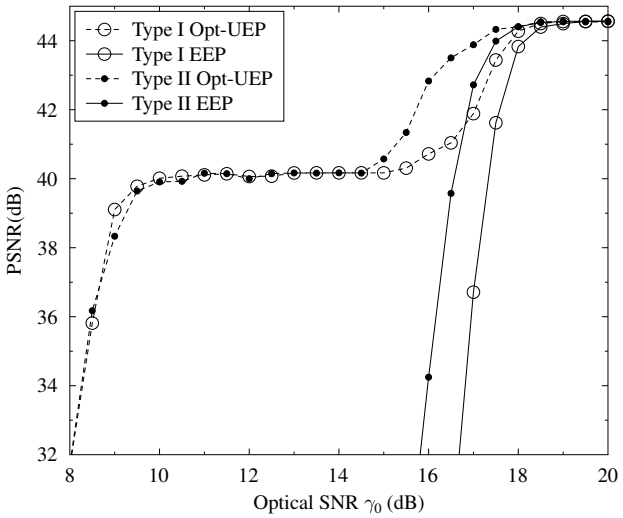


(c) PSNR vs optical SNR $\gamma_0$ for *Ice* with 16-HCSK-RSC

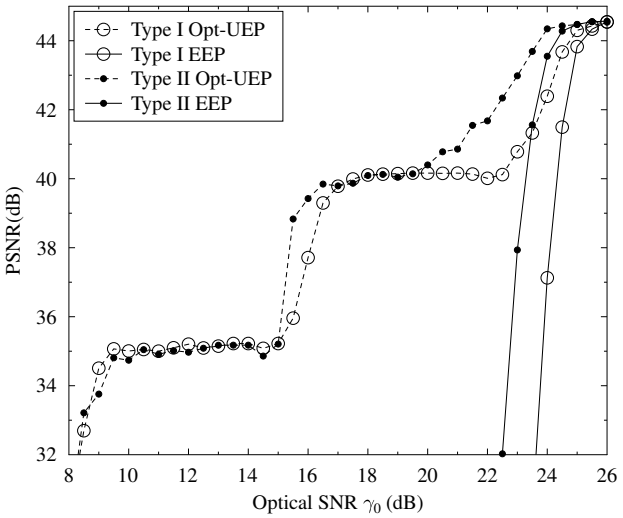


(d) PSNR vs optical SNR $\gamma_0$ for *Ice* with 64-HCSK-RSC

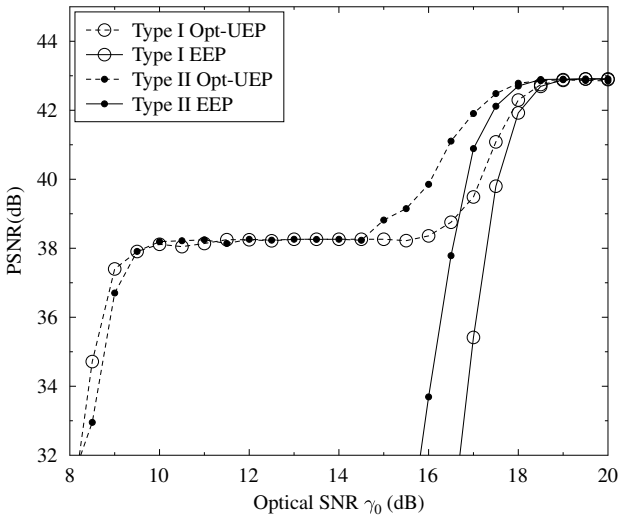


(e) PSNR vs optical SNR $\gamma_0$ for *Crew* with 16-HCSK-RSC

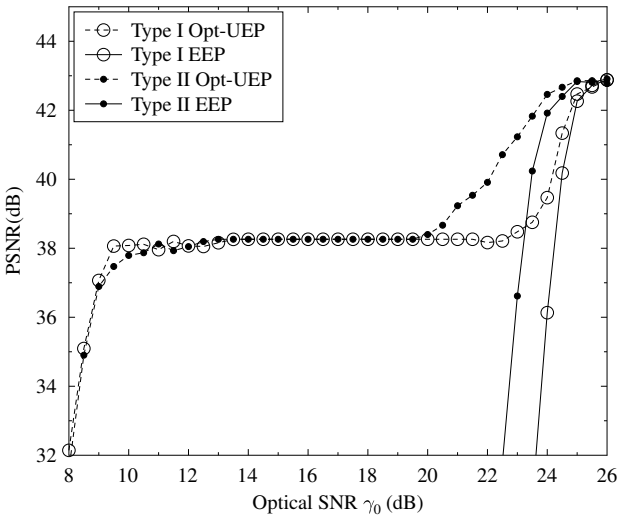


(f) PSNR vs optical SNR $\gamma_0$ for *Crew* with 64-HCSK-RSC

Figure 16: PSNR of Y components versus optical SNR $\gamma_0$ performance of our proposed optimised UEP 16/64-HCSK-RSC system, with either type I or type II HCSK are used as modulation.The EEP HCSK-RSC transmissions are used as benchmarks. The Soccer, Ice and Crew sequences are used for transmission over AWGN channels

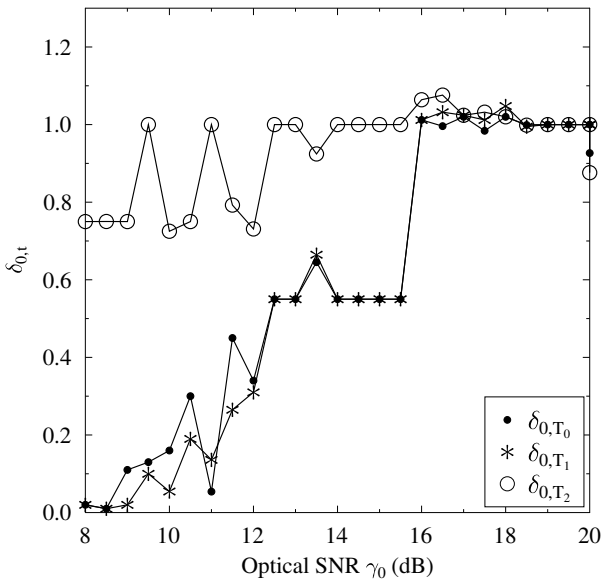


(a) The choice of $\delta_{0,t}$ vs optical SNR $\gamma_0$ for 16-HCSK-RSC

Figure 17: The choice of parameters versus optical SNR $\gamma_0$ with the optimised UEP 16-HCSK-RSC transmission system for the 1*st* video frame of *Soccer*

values, we will also characterise them at lower optical SNRs. A substantial gain can be observed for the UEP schemes in Fig. 16a around the PSNR of 36 $dB$. Quantitatively, up to 6.5 $dB$ of optical SNR reduction can be obtained by the optimised UEP system using the Type II constellation of Table VII, which is increased to 7.5 $dB$ for the optimised UEP systems using the Type I constellation. This energy reduction is an explicit benefit of the fact that the optimisation algorithm can decide whether to reduce the energy assigned to the less important layers depending on the channel conditions, owing to the design flexibility of M-HCSK. Once the channel becomes so noisy that it is unrealistic to transmit all the layers successfully, the optimisation will opt for reallocating the energy for transmitting the more important layers, by adjusting the $\delta_l$ values to increase the Euclidean distance amongst the 16-HCSK constellation subgroups conveying the base layer.

In Fig. 17a we can observe the choice of the optimum $\delta_{0,t}$ values versus the optical SNR $\gamma_0$ for the optimised UEP 16-HCSK-RSC transmission system for the 1*st* video frame of *Soccer*. We find that for the M-HCSK frame type $T_2$ $\delta_{0,T_2}$ stays close to 1 as $\gamma_0$ increases, which is due to the fact the frame type of $T_2$ happens to be $Lv_2 - Lv_2 - Lv_2$, hence there is no room for optimisation. By contrast, we can see that the values of $\delta_{0,t}$ for $T_0$ and $T_1$ are small at a low $\gamma_0$, in order to keep a reasonable minimum Euclidean distance for the lower-layer symbols, hence giving little priority to the higher layers. As $\gamma_0$ increases, the optimised $\delta_{0,t}$ values gradually settle around 1, as optimisation becomes unnecessary for high $\gamma_0$ values.

By contrast, the results recorded for the Soccer sequence with the aid of 64-HCSK are shown in Fig. 16b. We can observe that both UEP schemes associated with the Type I and Type II constellation outperformed their corresponding EEP counterparts. More specifically, when the Type II constellation design is adopted, the optimised UEP system outperforms its EEP benchmarker and achieves an optical SNR reduction of about 1.7 $dB$ at a PSNR of 37 $dB$. Similarly, for the Type I constellation design, the optimised UEP system achieves an optical SNR reduction of about 0.8 $dB$ at a PSNR of 37 $dB$. Additionally, it can be observed that the UEP schemes associated with the Type II HCSK constellation performs significantly better than that with the Type I HCSK, and an optical SNR reduction of about 1.9 $dB$ can be achieved at a PSNR of 37 $dB$ by using the former over the latter.

Similar trends can be observed, when the Ice or Crew sequences are used, as shown in Fig. 16c to Fig. 16f. We infer from these results that our optimised UEP M-HCSK-RSC scheme associated with the Type II constellation design is applicable to video sequences of diverse nature, and it is capable of achieving a beneficial performance gain for both $M = 16$ and 64. The subjective comparison of the decoded videos associated with our different regimes is discussed in Section V-F.

### *F. Subjective Comparison*

Explicitly, Fig. 19 shows the subjective comparison of the decoded video frames associated with our different regimes for 16-HCSK as the modulation using the Soccer sequence at an optical SNR value of $\gamma_0 = 10$ dB. The 20-th frame of the recovered videos of some of our schemes are shown in the top row of Fig. 19. The EEP 16-HCSK-RSC scheme using the Type I constellation is more error-prone according to Section V-E, and in this regime all three layers of this video frame failed to get recovered, and so did all their preceding frames. The difference frame, which is obtained by subtracting the recovered frame from the 20-th frame of the original video, has substantial non-zero values. Continuing from left to right, we can observe that the frames corresponding to the optimised UEP scheme using the Type I constellation, the EEP scheme using the Type II constellation and the optimised UEP scheme using the Type II constellation become sharper, revealing more intricate video details, while the corresponding difference frames have less and less non-zero values, which indicates the improvement of the video quality.

## VI. Conclusions

We conceived a hierarchical CSK modulation based on the traditional CSK, which is capable of conveying inter-dependent layers of video signals. Our scheme can be flexibly configured by changing its parameters. Furthermore, we provided a detailed design example for the employment of HCSK transmitting scalable video sources with the aid of the RSC code. An optimisation method is conceived in order to enhance the UEP and to improve the quality of the received video.

The simulation results of Fig. 16 show that the proposed system outperforms the traditional EEP scheme by about 1.7 dB of optical SNR at a peak signal-to-noise ratio (PSNR) of 37 dB, while it provides a wide range of system configurations providing optical SNR savings of up to 6.5 dB at a lower PSNR of 36 dB.

In our future work, we will consider the scenarios of joint FEC-modulation systems where the modulation and coding rate of FEC should be jointly optimized. We will also consider the hardware implementation of our VLC system.

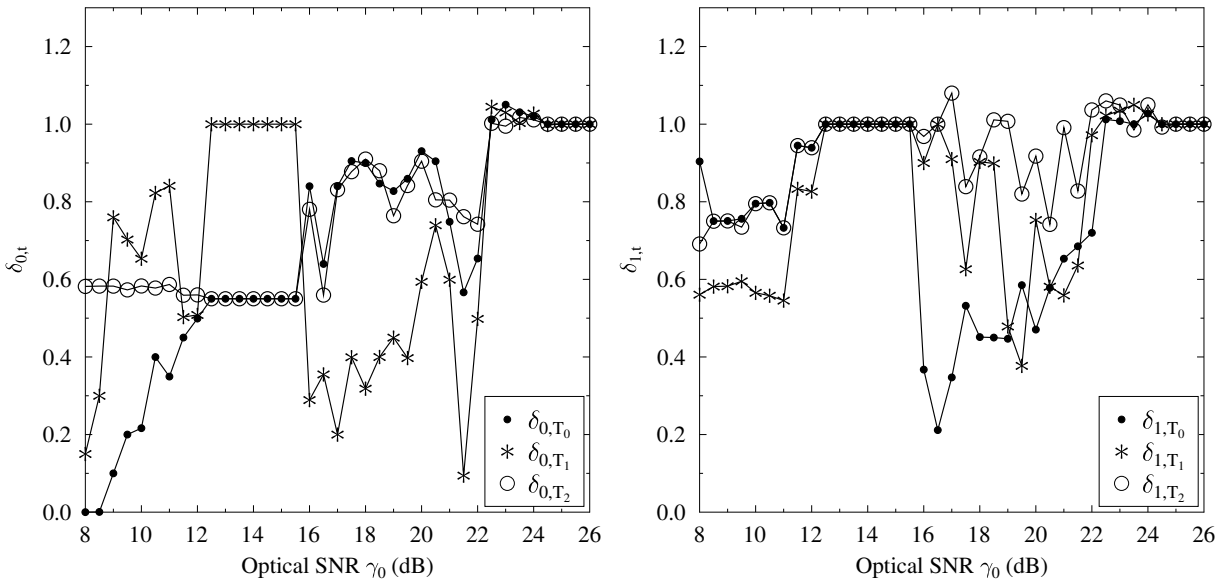


(a) The choice of $\delta_{0,t}$ vs optical SNR $\gamma_0$ for 64-HCSK-RSC

(b) The choice of $\delta_{1,t}$ vs optical SNR $\gamma_0$ for 64-HCSK-RSC

Figure 18: The choice of parameters versus optical SNR $\gamma_0$ with the optimised UEP 64-HCSK-RSC transmission system for the 1*st* video frame of *Soccer*

Figure 19: Comparison of decoded frames of the 20-th frame at an optical SNR $\gamma_0$ of 17 dB for the *Soccer* sequence with 16-HCSK adopted systems. The upper five columns (from left to right) indicate frames of the original video, the EEP 16-HCSK-RSC scheme using Type I constellation, the optimised UEP scheme using Type I constellation, the EEP scheme using Type II constellation, and the optimised UEP scheme using Type II constellation, respectively. The lower row correspond to the difference frames between the top ones and the original video frame.

## REFERENCES


[1] H. Burchardt, N. Serafimovski, D. Tsonev, S. Videv, and H. Haas, "VLC: Beyond point-to-point communication," *Communications Magazine, IEEE*, vol. 52, pp. 98–105, July 2014.

[2] T. Komine and M. Nakagawa, "Fundamental analysis for visible-light communication system using LED lights," *IEEE Transactions on Consumer Electronics*, vol. 50, pp. 100–107, February 2004.

[3] X. Li, J. Cucic, V. Jungnickel, and J. Armstrong, "On the capacity of intensity-modulated direct-detection systems and the information rate of ACO-OFDM for indoor optical wireless applications," *IEEE Transactions on Communications*, vol. 60, pp. 799–809, March 2012.

[4] T. Komine and M. Nakagawa, "Performance evaluation of visible-light wireless communication system using white LED lighting," in *International Symposium on Computers and Communications*, pp. 258–263, 2004.

[5] IEEE Computer Society, *IEEE Standard for Local and Metropolitan Area Networks - Part 15.7: Short-Range Wireless Optical Communication Using Visible Light*. 2011.

[6] K. Lee and H. Park, "Channel model and modulation schemes for visible light communications," in *IEEE International Midwest Symposium on Circuits and Systems*, pp. 1–3, 2011.

[7] G. Pang, T. Kwan, C.-H. Chan, and H. Liu, "LED traffic light as a communications device," in *1999 IEEE/IEEJ/JSAI International Conference on Intelligent Transportation Systems, 1999. Proceedings*, pp. 788–793.

[8] Y. Tanaka, S. Haruyama, and M. Nakagawa, "Wireless optical transmissions with white colored LED for wireless home links," in *The 11th IEEE International Symposium on Personal, Indoor and Mobile Radio Communications, 2000. PIMRC 2000*, vol. 2, pp. 1325–1329 vol.2.

[9] T. Komine and M. Nakagawa, "Integrated system of white LED visible-light communication and power-line communication," vol. 49, no. 1, pp. 71–79.

[10] "Visible Light Communications Consotium (VLCC)." http://www.vlcc.net/. (Visited on 12/02/2015).

[11] "JEITA / JEITA Standards / AV&IT Technology Standardization / Visible Light Communications." http://www.jeita.or.jp/. (Visited on 12/02/2015).

[12] "Home gigabit access project," in *[Online]. Available: http://www.ict-omega.eu/*, 2012.

[13] "St. Cloud first to sign on for new technology (Press release)." http://www.tmcnet.com/usubmit/2010/11/19/5148608.htm. (Visited on 12/02/2015).

[14] "Li-Fi Consortium." http://www.lificonsortium.org/. (Visited on 12/02/2015).

[15] "VLCA Visible Light Communications Association." http://vlca.net/. (Visited on 01/08/2016).

[16] B. Bai, Q. He, Z. Xu, and Y. Fan, "The color shift key modulation with non-uniform signaling for visible light communication," in *2012 1st IEEE International Conference on Communications in China Workshops (ICCC)*, pp. 37–42, Aug 2012.

[17] R. Drost and B. Sadler, "Constellation design for color-shift keying using billiards algorithms," in *2010 IEEE GLOBECOM Workshops (GC Wkshps)*, pp. 980–984, Dec 2010.

[18] R. Drost and B. Sadler, "Constellation design for channel precompensation in multi-wavelength visible light communications," *IEEE Transactions on Communications*, vol. 62, pp. 1995–2005, June 2014.

[19] R. Singh, T. O'Farrell, and J. David, "An enhanced color shift keying modulation scheme for high-speed wireless visible light communications," *Journal of Lightwave Technology*, vol. 32, pp. 2582–2592, July 2014.

[20] J. Jiang, Y. Huo, F. Jin, P. Zhang, Z. Wang, Z. Xu, H. Haas, and L. Hanzo, "Video streaming in the multiuser indoor visible light downlink," *IEEE Access*, vol. 3, pp. 2959–2986, 2015.

[21] E. Monteiro and S. Hranilovic, "Design and implementation of color-shift keying for visible light communications," *Journal of Lightwave Technology*, vol. 32, pp. 2053–2060, May 2014.

[22] J. Jiang, R. Zhang, and L. Hanzo, "Analysis and design of three-stage concatenated colour-shift keying," *IEEE Transactions on Vehicular Technology*, vol. PP, no. 99, pp. 1–1, 2015.

[23] J. G. Proakis and M. Salehi, *Digital Communications, 5th Edition*. McGraw-Hill, 2007.

[24] H. Sugiyama and K. Nosu, "MPPM: A method for improving the band-utilization efficiency in optical PPM," *IEEE Journal of Lightwave Technology*, vol. 7, pp. 1969–1979, March 1989.

[25] H. M. H. Shalaby, "Performance of uncoded overlapping PPM under communication constraints," in *IEEE International Communication Conference Proceeding*, (Geneva, Switzerland), pp. 512–516, May 1993.

[26] Z. Ghassemlooy, A. R. Hayes, N. L. Seed, and E. D. Kaluarachchi, "Digital pulse interval modulation for optical communications," *IEEE Communications Magazine*, vol. 36, pp. 95–99, December 1998.

[27] D. Shiu and J. M. Kahn, "Differential pulse-position modulation for power-efficient optical communication," *IEEE Transactions of Communications*, vol. 47, pp. 1201–1210, August 1999.

[28] T. Ohtsuki, "Multiple-subcarrier modulation in optical wireless communications," *IEEE Communications Magazine*, vol. 41, pp. 74–79, March 2003.

[29] Y. Fan and R. H. Green, "Comparison of pulse position modulation and pulse width modulation for application in optical communications," *Optics Engineering*, vol. 46, p. 065001, June 2007.

[30] T. T. Nguyen and L. Lampe, "Coded multipulse pulse-position modulation for free-space optical communications," *IEEE Transactions on Communications*, vol. 58, no. 4, pp. 1036–1041, 2010.

[31] J. Rufo, C. Quintana, F. Delgado, J. Rabadan, and R. Perez-Jimenez, "Considerations on modulations and protocols suitable for visible light communications (VLC) channels: Low and medium baud rate indoor visible ligth communications links," in *Consumer Communications and Networking Conference (CCNC), 2011 IEEE*, pp. 362–364, 2011.

[32] S. Arnon, "The effect of clock jitter in visible light communication applications," *Journal of Lightwave Technology*, vol. 30, no. 21, pp. 3434–3439, 2012.

[33] N. Fujimoto and H. Mochizuki, "477 Mbit/s visible light transmission based on OOK-NRZ modulation using a single commercially available visible LED and a practical LED driver with a pre-emphasis circuit," in *Optical Fiber Communication Conference and Exposition and the National Fiber Optic Engineers Conference (OFC/NFOEC), 2013*, pp. 1–3, 2013.

[34] H. Li, X. Chen, B. Huang, D. Tang, and H. Chen, "High bandwidth visible light communications based on a post-equalization circuit," *IEEE Photonics Technology Letters*, vol. 26, no. 2, pp. 119–122, 2014.

[35] S.-H. Chen and C.-W. Chow, "Color-shift keying and code-division multiple-access transmission for RGB-LED visible light communications using mobile phone camera," *IEEE Photonics Journal*, vol. 6, pp. 1–6, Dec 2014.

[36] M. Biagi, A. M. Vegni, S. Pergoloni, P. M. Butala, and T. D. C. Little, "Trace-orthogonal PPM-space time block coding under rate constraints for visible light communication," *IEEE Lightwave Technology*, vol. 33, pp. 481–494, January 2015.

[37] T. Zhang and Y. Xu, "Unequal packet loss protection for layered video transmission," *IEEE Transactions on Broadcasting*, vol. 45, pp. 243–252, June 1999.

[38] L. Zhang, G. Tech, K. Wegner, and S. Yea, "Test model 6 of 3D-HEVC and MV-HEVC," vol. N13940, ISO/IEC JTC-1/SC29/WG11, November 2013.

[39] H. Imaizumi and A. Luthra, *Three-Dimensional Television, Video and Display Technologies*, ch. MPEG-2 Multiview Profile, pp. 169–181. Berlin, Heidelberg, and New York: Springer Verlag, 2002.

[40] H. Schwarz, D. Marpe, and T. Wiegand, "Overview of the scalable video coding extension of the H.264/AVC standard," *IEEE Transactions on Circuits and Systems for Video Technology*, vol. 17, pp. 1103–1120, September 2007.

[41] Joint Video Team (JVT) of ISO/IEC MPEG and ITU-T VCEG, *ITU-T Rec. H.264/ISO/IEC 14496-10 AVC: Advanced Video Coding for Generic Audiovisual Services*, March 2010.

[42] A. Vetro, T. Wiegand, and G. Sullivan, "Overview of the stereo and multiview video coding extensions of the H.264/MPEG-4 AVC standard," *Proceedings of the IEEE*, vol. 99, pp. 626–642, April 2011.

[43] J. Boyce, W. Jang, D. Hong, S. Wenger, Y.-K. Wang, and Y. Chen, "High level syntax hooks for future extensions," in *JCT-VC document*, vol. JCTVC-H0388, (San JosÃ©, CA, USA), February 2012.

[44] A. Segall, "BoG report on SHVC," in *JCT-VC document*, vol. JCTVC-K0354, (Shanghai, China), October 2012.

[45] Y. Huo, M. El-Hajjar, and L. Hanzo, "Wireless video: An inter-layer error protection aided multi-layer approach," *IEEE Vehicular Technology Magazine*, submitted for publication.

[46] Y. Huo, X. Zuo, R. G. Maunder, and L. Hanzo, "Inter-layer FEC decoded multi-layer video streaming," in *IEEE Global Telecommunications Conference (GLOBECOM)*, (Anaheim, CA, USA), pp. 2113–2118, December 2012.

[47] Y. Huo, M. El-Hajjar, and L. Hanzo, "Inter-layer FEC aided unequal error protection for multilayer video transmission in mobile TV," *IEEE Transactions on Circuits and Systems for Video Technology*, vol. 23, pp. 1622–1634, September 2013.

[48] B. Masnick and J. Wolf, "On linear unequal error protection codes," *IEEE Transactions on Information Theory*, vol. 13, pp. 600–607, October 1967.

[49] D. Sejdinović, D. Vukobratović, A. Doufexi, V. Šenk, and R. Piechocki, "Expanding window fountain codes for unequal error protection," *IEEE Transactions on Communications*, vol. 57, pp. 2510–2516, November 2009.

[50] E. Maani and A. Katsaggelos, "Unequal error protection for robust streaming of scalable video over packet lossy networks," *IEEE Transactions on Circuits and Systems for Video Technology*, vol. 20, pp. 407–416, March 2010.

[51] S. Ahmad, R. Hamzaoui, and M. M. Al-Akaidi, "Unequal error protection using fountain codes with applications to video communication," *IEEE Transactions on Multimedia*, vol. 13, pp. 92–101, February 2011.

[52] K. Nguyen, T. Nguyen, and S.-C. Cheung, "Video streaming with network coding," *Journal of Signal Processing Systems*, vol. 59, pp. 319–333, June 2010.

[53] M. Halloush and H. Radha, "Network coding with multi-generation mixing: A generalized framework for practical network coding," *IEEE Transactions on Wireless Communications*, vol. 10, no. 2, pp. 466–473, 2011.

[54] P. Cataldi, M. Grangetto, T. Tillo, E. Magli, and G. Olmo, "Sliding-window raptor codes for efficient scalable wireless video broadcasting with unequal loss protection," *IEEE Transactions on Image Processing*, vol. 19, pp. 1491–1503, June 2010.

[55] C. Hellge, D. Gomez-Barquero, T. Schierl, and T. Wiegand, "Layer-aware forward error correction for mobile broadcast of layered media," *IEEE Transactions on Multimedia*, vol. 13, pp. 551–562, June 2011.

[56] N. Thomos, J. Chakareski, and P. Frossard, "Prioritized distributed video delivery with randomized network coding," *IEEE Transactions on Multimedia*, vol. 13, pp. 776–787, Aug 2011.

[57] F. Marx and J. Farah, "A novel approach to achieve unequal error protection for video transmission over 3G wireless networks," *Signal Processing: Image Communication*, vol. 19, no. 4, pp. 313–323, 2004.

[58] S. X. Ng, J. Y. Chung, and L. Hanzo, "Turbo-detected unequal protection MPEG-4 wireless video telephony using multi-level coding, trellis coded modulation and space-time trellis coding," *IEE Proceedings Communications*, vol. 152, pp. 1116–1124, December 2005.

[59] M. Aydinlik and M. Salehi, "Turbo coded modulation for unequal error protection," *IEEE Transactions on Communications*, vol. 56, pp. 555–564, April 2008.

[60] Y. C. Chang, S. W. Lee, and R. Komiya, "A fast forward error correction allocation algorithm for unequal error protection of video

transmission over wireless channels," *IEEE Transactions on Consumer Electronics*, vol. 54, pp. 1066–1073, August 2008.

[61] Y. C. Chang, S. W. Lee, and R. Komiya, "A low complexity hierarchical QAM symbol bits allocation algorithm for unequal error protection of wireless video transmission," *IEEE Transactions on Consumer Electronics*, vol. 55, pp. 1089–1097, August 2009.

[62] Nasruminallah and L. Hanzo, "Near-capacity H.264 multimedia communications using iterative joint source-channel decoding," *IEEE Communications Surveys and Tutorials*, vol. 14, pp. 538–564, Second Quarter 2012.

[63] Nasruminallah, M. El-Hajjar, N. Othman, A. Quang, and L. Hanzo, "Over-complete mapping aided, soft-bit assisted iterative unequal error protection H.264 Joint source and channel decoding," in *Vehicular Technology Conference, 2008. VTC 2008-Fall. IEEE 68th*, pp. 1–5, 2008.

[64] H. Wang, F. Zhai, Y. Eisenberg, and A. Katsaggelos, "Cost-distortion optimized unequal error protection for object-based video communications," *IEEE Transactions on Circuits and Systems for Video Technology*, vol. 15, pp. 1505–1516, December 2005.

[65] H. Ha and C. Yim, "Layer-weighted unequal error protection for scalable video coding extension of H.264/AVC," *IEEE Transactions on Consumer Electronics*, vol. 54, pp. 736–744, May 2008.

[66] D. Vukobratović, V. Stanković, D. Sejdinović, L. Stanković, and Z. Xiong, "Scalable video multicast using expanding window fountain codes," *IEEE Transactions on Multimedia*, vol. 11, no. 6, pp. 1094–1104, 2009.

[67] D. Wu, Y. T. Hou, and Y.-Q. Zhang, "Transporting real-time video over the Internet: challenges and approaches," *Proceedings of the IEEE*, vol. 88, pp. 1855–1877, December 2000.

[68] T. Stockhammer, M. Hannuksela, and T. Wiegand, "H.264/AVC in wireless environments," *IEEE Transactions on Circuits and Systems for Video Technology*, vol. 13, pp. 657–673, July 2003.

[69] C. Zhu, Y. Huo, B. Zhang, R. Zhang, M. El-Hajjar, and L. Hanzo, "Adaptive truncated HARQ aided layered video streaming relying on inter-layer FEC coding," *IEEE Transactions on Vehicular Technology*, vol. PP, no. 99, pp. 1–1, 2015.

[70] B. Masnick and J. Wolf, "On linear unequal error protection codes," *IEEE Transactions on Information Theory*, vol. 13, pp. 600–607, October 1967.

[71] J. Hagenauer, "Rate-compatible puncture convolutional codes (RCPC) and their application," *IEEE Transactions on Communications*, vol. 36, pp. 389–400, April 1988.

[72] A. Calderbank and N. Seshadri, "Multilevel codes for unequal error protection," *IEEE Transactions on Information Theory*, vol. 39, pp. 1234–1248, Jul 1993.

[73] A. Albanese, J. Blomer, J. Edmonds, M. Luby, and M. Sudan, "Priority encoding transmission," *IEEE Transactions on Information Theory*, vol. 42, pp. 1737–1744, November 1996.

[74] P. Chou, A. Mohr, A. Wang, and S. Mehrotra, "Error control for receiver-driven layered multicast of audio and video," *IEEE Transactions on Multimedia*, vol. 3, pp. 108–122, March 2001.

[75] Q. Zhang, W. Zhu, and Y.-Q. Zhang, "Channel-adaptive resource allocation for scalable video transmission over 3G wireless network," *IEEE Transactions on Circuits and Systems for Video Technology*, vol. 14, pp. 1049–1063, August 2004.

[76] T. Brüggen and P. Vary, "Unequal error protection by modulation with unequal power allocation," *IEEE Communications Letters*, vol. 9, pp. 484–486, June 2005.

[77] B. Barmada, M. Ghandi, E. Jones, and M. Ghanbari, "Prioritized transmission of data partitioned H.264 video with hierarchical QAM," *IEEE Signal Processing Letters*, vol. 12, pp. 577–580, Aug 2005.

[78] Y. C. Chang, S. W. Lee, and R. Komiya, "A low-complexity unequal error protection of H.264/AVC video using adaptive hierarchical QAM," *IEEE Transactions on Consumer Electronics*, vol. 52, pp. 1153–1158, Nov 2006.

[79] N. Rahnavard, H. Pishro-Nik, and F. Fekri, "Unequal error protection using partially regular LDPC codes," *IEEE Transactions on Communications*, vol. 55, pp. 387–391, March 2007.

[80] J. Park, H. Lee, S. Lee, and A. Bovik, "Optimal channel adaptation of scalable video over a multicarrier-based multicell environment," *IEEE Transactions on Multimedia*, vol. 11, pp. 1062–1071, October 2009.

[81] P. Li, Y. Chang, N. Feng, and F. Yang, "A novel hierarchical QAM-based unequal error protection scheme for H.264/AVC video over frequency-selective fading channels," *IEEE Transactions on Consumer Electronics*, vol. 56, pp. 2741–2746, November 2010.

[82] S. S. Arslan, P. C. Cosman, and L. B. Milstein, "Coded hierarchical modulation for wireless progressive image transmission," *IEEE Transactions on Vehicular Technology*, pp. 4299 – 4313, Nov. 2011.

[83] A. A. Khalek, C. Caramanis, and R. W. Heath, "A cross-layer design for perceptual optimization of H.264/SVC with unequal error protection," *IEEE Journal on Selected Areas in Communications*, vol. 30, no. 7, pp. 1157–1171, 2012.

[84] S.-H. Chang, M. Rim, P. Cosman, and L. Milstein, "Optimized unequal error protection using multiplexed hierarchical modulation," *IEEE Transactions on Information Theory*, vol. 58, pp. 5816–5840, Sept 2012.

[85] K. M. Alajel, W. Xiang, and Y. Wang, "Unequal error protection scheme based hierarchical 16-QAM for 3-D video transmission," *IEEE Transactions on Consumer Electronics*, vol. 58, no. 3, pp. 731–738, 2012.

[86] Y. Wu, S. Kumar, F. Hu, Y. Zhu, and J. Matyjas, "Cross-layer forward error correction scheme using raptor and RCPC codes for prioritized video transmission over wireless channels," *IEEE Transactions on Circuits and Systems for Video Technology*, vol. 24, pp. 1047–1060, June 2014.

[87] T. Nguyen, P. Cosman, and L. Milstein, "Double-layer video transmission over decode-and-forward wireless relay networks using hierarchical modulation," *IEEE Transactions on Image Processing*, vol. 23, pp. 1791–1804, April 2014.

[88] L.-F. Wei, "Coded modulation with unequal error protection," *IEEE Transactions on Communications*, vol. 41, pp. 1439–1449, Oct 1993.

[89] S. Gadkari and K. Rose, "Time-division versus superposition coded modulation schemes for unequal error protection," *IEEE Transactions on Communications*, vol. 47, pp. 370–379, Mar 1999.

[90] M. Isaka, M. Fossorier, R. Morelos-Zaragoza, S. Lin, and H. Imai, "Multilevel coded modulation for unequal error protection and multistage decoding. II. asymmetric constellations," *IEEE Transactions on Communications*, vol. 48, pp. 774–786, May 2000.

[91] R. Morelos-Zaragoza, M. Fossorier, S. Lin, and H. Imai, "Multilevel coded modulation for unequal error protection and multistage decoding .i. symmetric constellations," *IEEE Transactions on Communications*, vol. 48, pp. 204–213, Feb 2000.

[92] J. Kim and G. Pottie, "Unequal error protection tcm codes," *IEE Proceedings-Communications*, vol. 148, pp. 265–272, Oct 2001.

[93] M. Zamkotsian, K. Peppas, F. Lazarakis, and P. Cottis, "Multilevel spatial hierarchical modulation: An efficient scheme for unequal error protection under rician fading," *IEEE Transactions on Vehicular Technology*, vol. PP, no. 99, pp. 1–1, 2014.

[94] R. Chang, S.-J. Lin, and W.-H. Chung, "Hierarchical space shift keying for unequal error protection," *IEEE Communications Letters*, vol. 16, pp. 1341–1344, September 2012.

[95] S. Arslan, P. Cosman, and L. Milstein, "Coded hierarchical modulation for wireless progressive image transmission," *IEEE Transactions on Vehicular Technology*, vol. 60, pp. 4299–4313, Nov 2011.

[96] Y. Noh, H. Lee, W. Lee, and I. Lee, "Design of unequal error protection for MIMO-OFDM systems with hierarchical signal constellations," *Journal of Communications and Networks*, vol. 9, pp. 167–176, June 2007.

[97] T. Quazi and H. Xu, "Simple unequal error protection mechanism for multimedia traffic using the Alamouti structure with hierarchical modulation and signal space diversity," *IET Communications*, vol. 8, no. 17, pp. 3128–3135, 2014.

[98] H. Nguyen, H. Nguyen, and T. Le-Ngoc, "Signal transmission with unequal error protection in wireless relay networks," *IEEE Transactions on Vehicular Technology*, vol. 59, pp. 2166–2178, June 2010.

[99] M. Morimoto, M. Okada, and S. Komaki, "Joint on-board resource sharing and hierarchical modulation scheme for satellite communication," in *Global Telecommunications Conference, 1995. GLOBECOM '95., IEEE*, vol. 3, pp. 1662–1666, 1995.

[100] M. Morimoto, M. Okada, and S. Komaki, "A hierarchical image transmission system for multimedia mobile communication," in *Wireless Image/Video Communications, 1996., First International Workshop on*, pp. 80–84, 1996.

[101] J. Hossain, P. K. Vitthaladevuni, M. S. Alouini, and V. K. Bhargava, "Adaptive hierarchical modulation for simultaneous voice and multiclass data transmission over fading channels," *IEEE Transactions on Vehicular Technology*, vol. 55, pp. 1181–1194, Jul. 2006.

[102] M. K. Chang and S. Y. Lee, "Performance analysis of cooperative communication system with hierarchical modulation over Rayleigh fading channel," *IEEE Transactions on Wireless Communications*, vol. 8, pp. 2848–2852, Jun. 2009.

[103] H. Sun, S. X. Ng, C. Dong, and L. Hanzo, "Decode-and-forward cooperation-aided triple-layer turbo-trellis-coded hierarchical modulation," *Communications, IEEE Transactions on*, vol. 63, pp. 1136–1148, April 2015.

[104] C. Hellge, S. Mirta, T. Schierl, and T. Wiegand, "Mobile TV with SVC and hierarchical modulation for DVB-H broadcast services," *IEEE International Symposium on Broadband Multimedia Systems and Broadcasting, 2009. BMSB '09.*, pp. 1–5, May. 2009.

[105] ETSI, *Digital Video Broadcasting (DVB); Framing structure, channel coding and modulation for digital terrestrial television*, August 1997. EN 300 744 V1.1.2.
[106] H. Sun, C. Dong, S. Ng, and L. Hanzo, "Five decades of hierarchical modulation and its benefits in relay-aided networking," *IEEE Access*, vol. 3, pp. 2891–2921, 2015.
[107] L. Hanzo and P. Cherriman and J. Streit, "Wireless Video Communications: From Second to Third Generation Systems, WLANs and Beyond." IEEE Press, 2001. (For detailed contents please refer to http://www-mobile.ecs.soton.ac.uk.).
[108] D. Karunatilaka, F. Zafar, V. Kalavally, and R. Parthiban, "LED based indoor visible light communications: State of the art," *IEEE Communications Surveys and Tutorials*, vol. 17, pp. 1649–1678, Aug. 2015.
[109] Sony, "F55 CineAlta 4K the future, ahead of schedule." http://pro.sony.com/bbsccms/assets/files/show/highend/pdf/F55_Camera.pd 2012. Retrieved on 15/02/2016.
[110] Y. Hong, J. Chen, Z. Wang, and C. Yu, "Performance of a precoding MIMO system for decentralized multiuser indoor visible light communications," *IEEE Photonics Journal*, vol. 5, August 2013.
[111] M. F. Guerra-Medina, O. González, B. Rojas-Guillama, J. A. Martín-González, F. Delgado, and J. Rabadán, "Ethernet-OCDMA system for multi-user visible light communications," *Electronics Letters*, vol. 48, pp. 227–228, Feb. 2012.
[112] M. Jafar, D. C. O'Brien, C. J. Stevens, and D. J. Edwards, "Evaluation of coverage area for a wide line-of-sight indoor optical free-space communication system employing coherent detection," *IET Communications*, vol. 2, pp. 18–26, Jan. 2008.
[113] C. CIE, "Commission internationale de l'eclairage proceedings, 1931," 1932.
[114] Y. Huo, M. El-Hajjar, R. Maunder, and L. Hanzo, "Layered wireless video relying on minimum-distortion inter-layer FEC coding," *IEEE Transactions on Multimedia*, vol. 16, pp. 697–710, April 2014.
[115] H. Xiao, Q. Dai, X. Ji, and W. Zhu, "A novel JSCC framework with diversity-multiplexing-coding gain tradeoff for scalable video transmission over cooperative MIMO," *IEEE Transactions on Circuits and Systems for Video Technology*, vol. 20, pp. 994–1006, July 2010.
[116] Q. Zhang, W. Zhu, and Y.-Q. Zhang, "Channel-adaptive resource allocation for scalable video transmission over 3G wireless network," *IEEE Transactions on Circuits and Systems for Video Technology*, vol. 14, pp. 1049–1063, August 2004.
[117] D. Jurca, P. Frossard, and A. Jovanovic, "Forward error correction for multipath media streaming," *IEEE Transactions on Circuits and Systems for Video Technology*, vol. 19, pp. 1315–1326, September 2009.
[118] R. Hamzaoui, V. Stankovic, and Z. Xiong, "Optimized error protection of scalable image bit streams [advances in joint source-channel coding for images]," *IEEE Signal Processing Magazine*, vol. 22, pp. 91–107, Nov. 2005.
[119] N. Thomos, J. Chakareski, and P. Frossard, "Prioritized distributed video delivery with randomized network coding," *IEEE Transactions on Multimedia*, vol. 13, pp. 776–787, Aug. 2011.
[120] D. Vukobratovic, V. Stankovic, D. Sejdinovic, L. Stankovic, and Z. Xiong, "Scalable video multicast using expanding window fountain codes," *IEEE Transactions on Multimedia*, vol. 11, pp. 1094–1104, Oct. 2009.
[121] P. Cataldi, M. Grangetto, T. Tillo, E. Magli, and G. Olmo, "Sliding-window raptor codes for efficient scalable wireless video broadcasting with unequal loss protection," *IEEE Transactions on Image Processing*, vol. 19, pp. 1491–1503, June 2010.
[122] E. Maani and A. K. Katsaggelos, "Unequal error protection for robust streaming of scalable video over packet lossy networks," *IEEE Transactions on Circuits and Systems for Video Technology*, vol. 20, pp. 407–416, Mar. 2010.
[123] Z. Wu, A. Bilgin, and M. W. Marcellin, "Joint source/channel coding for image transmission with JPEG2000 over memoryless channels," *IEEE Transactions on Image Processing*, vol. 14, pp. 1020–1032, Aug. 2005.
[124] H. Ha and C. Yim, "Layer-weighted unequal error protection for scalable video coding extension of H.264/AVC," *IEEE Transactions on Consumer Electronics*, vol. 54, pp. 736–744, May 2008.
[125] "Find minimum of constrained nonlinear multivariable function using matlab fmincon." http://uk.mathworks.com/help/optim/ug/fmincon.html. (Accessed on 04/22/2016).
[126] L. Hanzo, P. Cherriman, and J. Streit, *Video Compression and Communications: From Basics to H.261, H.263, H.264, MPEG2, MPEG4 for DVB and HSDPA-Style Adaptive Turbo-Transceivers*. New York: John Wiley, 2007.
[127] A. Detti, G. Bianchi, C. Pisa, F. S. Proto, P. Loreti, W. Kellerer, S. Thakolsri, and J. Widmer, "SVEF: an open-source experimental evaluation framework for H.264 scalable video streaming," in *IEEE Symposium on Computers and Communications, ISCC*, (Sousse, Tunisia), pp. 36–41, July 2009.
[128] Y. Guo, Y. Chen, Y. K. Wang, H. Li, M. M. Hannuksela, and M. Gabbouj, "Error resilient coding and error concealment in scalable video coding," *IEEE Transactions on Circuits and Systems for Video Technology*, vol. 19, pp. 781–795, June 2009.
[129] Y. Chen, K. Xie, F. Zhang, P. Pandit, and J. Boyce, "Frame loss error concealment for svc," *Journal of Zhejiang University SCIENCE A*, vol. 7, pp. 677–683, May 2006.

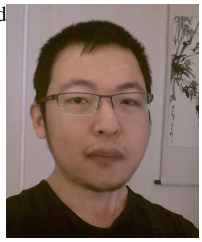

**Chuan Zhu** received the B.Eng. degree from Southeast University, Nanjing, China, and the M.Sc. degree (with distinction) in radio-frequency communication systems from the University of Southampton, Southampton, U.K., in 2010. He is currently working toward the Ph.D. degree with the Communications Research Group, School of Electronics and Computer Science, University of Southampton. His research interests include joint source–channel decoding, video compression and transmission, and extrinsic information transfer chart-aided turbo detection, as well as cooperative communications. Mr. Zhu received the Student Case Award toward his Ph.D. study from British Telecom, London, U.K.

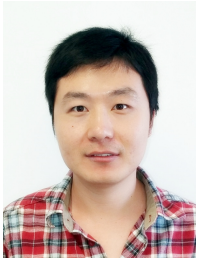

**Yongkai Huo** received the B.Eng. degree with distinction in computer science and technology from Hefei University of Technology, Hefei, China, in 2006 and the M.Eng. degree in computer software and theory from University of Science and Technology of China, Hefei, China, in 2009. In 2014, he was awarded a Ph.D in Wireless Communications group, School of Electronics and Computer Science, University of Southampton, Southampton, UK, where he is currently working as a research fellow. He received a scholarship under the China-U.K. Scholarships for Excellence Programme. His research interests include distributed video coding, multiview video coding, robust wireless video streaming and joint source-channel decoding.

**Junyi Jiang** received his BEng degree in communication engineering from Heilongjiang Institute of Science and Technology, PRC, in 2009 and his MSc degree with distinction in wireless communication from the University of Southampton, UK, in 2010. He is currently working towards the PhD degree with the Wireless Group, the University of Southampton, UK.

His research interests include indoor visible light communication, free-space optical communication and iterative detection.

**Hua Sun** received the B.Eng. degree in electronics and information engineering from the Huazhong University of Science & Technology (HUST), Wuhan, China, in 2009. In 2010, he obtained a MSc degree with distinction in Wireless Communications from the University of Southampton, Southampton, UK. He is currently working towards the PhD degree in the Research Group of Communications, Signal Processing and Control, School of Electronics and Computer Science, University of Southampton, Southampton, UK. His research interests include Superposition Modulation, Hierarchical Modulation, Turbo Trellis-Coded Modulation as well as cooperative communications.

**Chen Dong** received his BS degree in electronic information sciences and technology from University of Science and Technology of China(USTC), Hefei, China in 2004, and his MEng degree in pattern recognition and automatic equipment from the University of Chinese Academy of Sciences, Beijing, China in 2007. In 2014, he was awarded PhD degree from the University of Southampton, UK. Now he is a post-doc in the same University. He was the recipient of scholarship under the UK-China Scholarships for Excellence programme and he has been awarded Best Paper Award at IEEE VTC 2014-Fall. His research interests include applied math, relay system, channel modelling and cross-layer optimization.

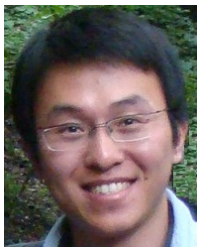

**Rong Zhang** (M'09) received his PhD (Jun 09) from Southampton University, UK and his BSc (Jun 03) from Southeast University, China. Before doctorate, he was an engineer (Aug 03-July 04) at China Telecom and a research assistant (Jan 06-May 09) at Mobile Virtual Center of Excellence (MVCE), UK. After being a post-doctoral researcher (Aug 09-July 12) at Southampton University, he took industrial consulting leave (Aug 12-Jan 13) for Huawei Sweden R& D as a system algorithms specialist. Since Feb 13, he has been appointed as a lecturer at CSPC group of ECS, Southampton University. He has 40+ journals in prestigious publication avenues (e.g. IEEE, OSA) and many more in major conference proceedings. He regularly serves as reviewer for IEEE transactions/journals and has been several times as TPC member/invited session chair of major conferences. He is the recipient of joint funding of MVCE and EPSRC and is also a visiting researcher under Worldwide University Network (WUN). More details can be found at http://www.ecs.soton.ac.uk/people/rz

**Lajos Hanzo** FREng, FIEEE, FIET, Fellow of EURASIP, DSc received his degree in electronics in 1976 and his doctorate in 1983. In 2009 he was awarded the honorary doctorate "Doctor Honoris Causa" by the Technical University of Budapest. During his 38-year career in telecommunications he has held various research and academic posts in Hungary, Germany and the UK. Since 1986 he has been with the School of Electronics and Computer Science, University of Southampton, UK, where he holds the chair in telecommunications. He has successfully supervised about 100 PhD students, co-authored 20 John Wiley/IEEE Press books on mobile radio communications totalling in excess of 10 000 pages, published 1500+ research entries at IEEE Xplore, acted both as TPC and General Chair of IEEE conferences, presented keynote lectures and has been awarded a number of distinctions. Currently he is directing a 100-strong academic research team, working on a range of research projects in the field of wireless multimedia communications sponsored by industry, the Engineering and Physical Sciences Research Council (EPSRC) UK, the European Research Council's Advanced Fellow Grant and the Royal Society's Wolfson Research Merit Award. He is an enthusiastic supporter of industrial and academic liaison and he offers a range of industrial courses. He is also a Governor of the IEEE VTS. During 2008 - 2012 he was the Editor-in-Chief of the IEEE Press and a Chaired Professor also at Tsinghua University, Beijing. His research is funded by the European Research Council's Senior Research Fellow Grant. For further information on research in progress and associated publications please refer to http://www-mobile.ecs.soton.ac.uk Lajos has 24 000 citations.